Journal of Geography and Geology; Vol. 6, No. 2; 2014
ISSN 1916-9779 E-ISSN 1916-9787
Published by Canadian Center of Science and Education

Late Holocene Geomorphology of the Columbia River Estuary, Oregon and Washington, USA

Curt Peterson[1], Sandy Vanderburgh[2] & Michael C. Roberts[3]

[1] Geology Department, Portland State University, Portland, USA

[2] Lethbridge College, Centre for Applied Arts and Sciences, 3000 College Drive South, Lethbridge, AB, T1K 1L6, Canada

[3] Simon Fraser University, 8888 University Drive, Burnaby B.C., V5A 1S6, Canada

Correspondence: Curt Peterson, Geology Department, Portland State University, Portland, USA. Tel: 1-503-725-3375. E-mail: curt.d.peterson@gmail.com

Received: January 13, 2014 Accepted: February 7, 2014 Online Published: March 31, 2014

doi:10.5539/jgg.v6n2p1 URL: http://dx.doi.org/10.5539/jgg.v6n2p1

Abstract

Abundant river sediment supply and an open-water central bay area characterize the geomorphology of the large Columbia River estuary (~ 100 km in length). Lateral floodplains and marsh islands do constrict the uppermost reaches of the estuary, but the central axes of the lower estuary are dominated by shallow sand shoals (0–4 m water depth). A total of 58 vibracores are used to document the grain size and age (0–2,500 ^{14}CyrBP) of late Holocene deposits in the estuary. Sedimentation rates in stable floodplains (1.1 m ka^{-1}) reflect rates of relative sea level rise (0.75 m ka^{-1}). Sedimentation rates of muddy sand accretionary banks and prehistoric sand shoals (1.5–7 m ka^{-1}) greatly exceed coeval rates of sea level rise, so they must represent short–term rates of vertical accretion resulting from channel lateral migration and associated cut and fill processes. The apparent paradox of unfilled accommodation space in the estuary is resolved by 1) winter wind–wave erosion of sand shoals to -3 m NAVD88 elevation and 2) asymmetric fluvial-tidal advection that results in net seaward transport of bed load in shallow tidal channels (> – 10 m NAVD88) and shallow subtidal shoals (> – 4 m NAVD88) during spring river flooding.

Keywords: fluvial-tidal, estuary, late Holocene, sedimentation rates, sediment transport

1. Introduction

The extensive Columbia River estuary (~ 100 km in length) provides a geomorphic paradox. The submerged incised river valley is abundantly supplied with river sediment (10–15 million tons per year) (Sherwood & Creager, 1990). The river mouth lacks a delta and the shallow estuary has not completely in–filled with tidal marshes or floodplains (Figure 1). The lack of a deep central bay in the Columbia River estuary is consistent with a high throughput of bed load (Gates, 1994; Baker et al., 2010) during late Holocene time. However, latest Holocene infilling of the central bay did not reach completion, as demonstrated by 1) the lack of substantial lateral floodplain development and 2) the presence of an open-water central bay that extends 30 km upriver of the tidal inlet. The open bay reaches of the estuary contrast with extensive flood plain constriction in the upriver sections of the lower Columbia River valley, which extends another 100 km upriver to the modern head of tide in the Cascade Range Gorge (Peterson et al., 2014).

The expanse of open water in the central bay of the Columbia River estuary (Figure 1) appears to imply the availability of accommodation space (Dalrymple et al., 1994) for new sediment accumulation in the estuary. These conditions, therefore, likely encouraged interpretations that the lower estuary serves as a net sink for littoral sand entering the river mouth in deep channels (Walter, 1980; Sherwood & Creager, 1990). However, long-term declines in sedimentation rates from mid-Holocene to late-Holocene time in the lower Columbia River valley (Peterson et al., 2013) demonstrate substantial bypassing of river sand (about 5 million cubic meters per year) to the Pacific Ocean. The Holocene depositional filling of the inner-shelf (Twichell et al., 2010) and the late Holocene progradation of barrier beach plains on either sides of the Columbia River mouth (Vanderburgh et al., 2010) are attributed to the substantial throughput of bed load from the Columbia River to the marine side (Peterson et al., 2010).

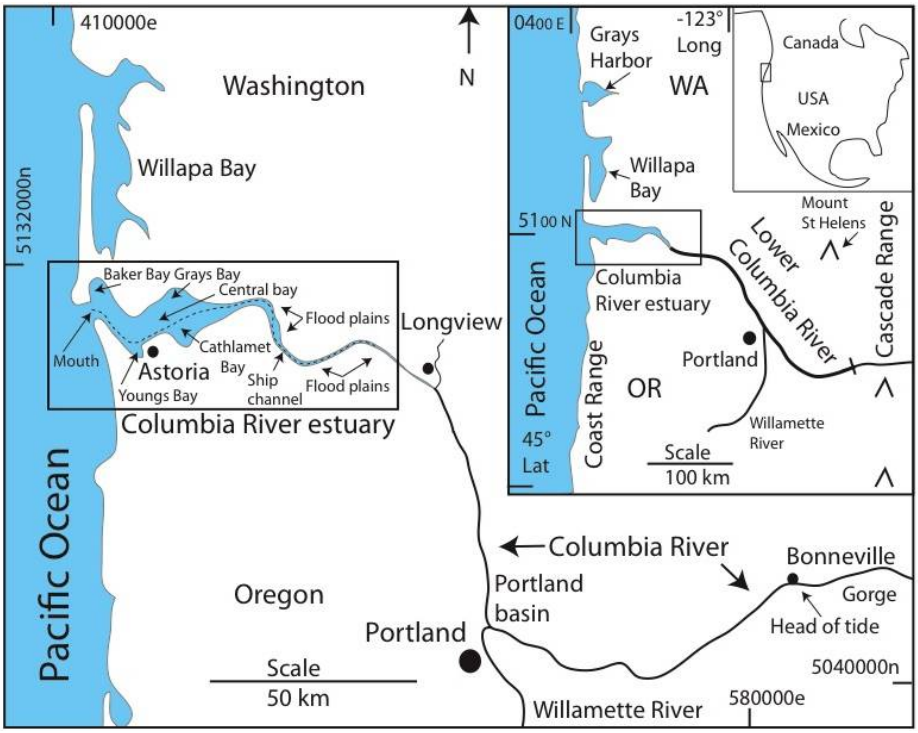

Figure 1. Location of the Columbia river estuary

The estuary (boxed, 100 km in length) occurs in the lower Columbia River valley, which serves as the border between Washington and Oregon States. The antecedent river valley is tidally influenced from the mouth at Astoria, OR to the present head of tide at Bonneville, WA, totaling a river distance of 225 km.

The goals of this paper are to reconcile the apparent opposing prehistoric conditions of 1) high supply rates of Columbia River sediment to the Columbia River estuary with 2) a general lack of intertidal marsh islands or laterally accreting supratidal floodplains in the central axes of the lower estuary (Figure 1). A total of 58 vibracores (4–6 m depth) are used to establish the deposit grain sizes and sedimentation rates in the estuary during latest Holocene time (0–2.5 ka). Early historic bathymetric surveys of the estuary are utilized together with wind–wave fetch to calculate bottom orbital velocities in the central axes of the middle and lower estuarine reaches. Early historic conditions of tidal, fluvial, and wind–wave forcing in the estuary are used to develop a conceptual model of bed load bypassing through the estuary to the Pacific Ocean in latest Holocene time. The unusual geomorphic development of the Columbia River estuary is relevant to regional sediment management in the bi-state region (Gelfenbaum & Kaminsky, 2010), and more broadly, to the modeling of bed load dynamics in shallow estuaries that are influenced by 1) high-rates of river sediment supply, 2) fluvial-tidal flow regimes, and 3) very–high wind–wave energies.

2. Background

As a major shipping route the lower Columbia River (Figure 1) has been systematically surveyed for bathymetry since at least 1839 (Hickson & Rudolf, 1951). Historic bathymetric change maps were compiled by CREDDP (1983) to establish potential erosion or accretion following 1) wide–scale impoundments of the Columbia River and its tributaries (1937–present), 2) long-term impacts of repeated jetty construction in the Columbia River mouth (1905-present), and 3) extensive deepening and channel bank stabilization of the Columbia River ship channel (1903–present) (Simenstad et al., 1990; Sherwood et al., 1990; Byrnes & Li, 1998). The CREDEP bathymetric change maps (CREDDP, 1983) were utilized in this research to select core site locations that were not directly impacted by channel dredging and/or stabilization. Most recently, light detection and ranging radar (LiDAR) has been used to map the intertidal deposit elevations in the Columbia River estuary (Pugetsoundlidar, 2013). The LiDAR data were used in this study to establish core site elevations relative to the NAVD88 elevation datum.

Bathymetric and hydrographic surveys near the mouth of the Columbia River (Hickson & Rudolf, 1951) demonstrate the presence of a shallow central bay since earliest–historic time in 1792 (Figure 2). North and

south channels (~ 8–15 m water depth) dissected shallow sand shoals (< 5 m depth) that extended to within several kilometers of the tidal inlet. The main channel at the Columbia River mouth stabilized since the onset of jetty construction, beginning at the turn of the last century (circa 1902). During early historic time (1792–1885) the north and south tidal channels generally decreased in depth from the mouth (10–15 m depth) the south channel at the Port of Astoria (to 8–12 m depth), a distance of about 20 km from the mouth. The narrow south channel (~ 500 m width) was artificially deepened during the 1900s to enable the passage of large ships to upriver ports at the Port of Portland, OR (Figure 1).

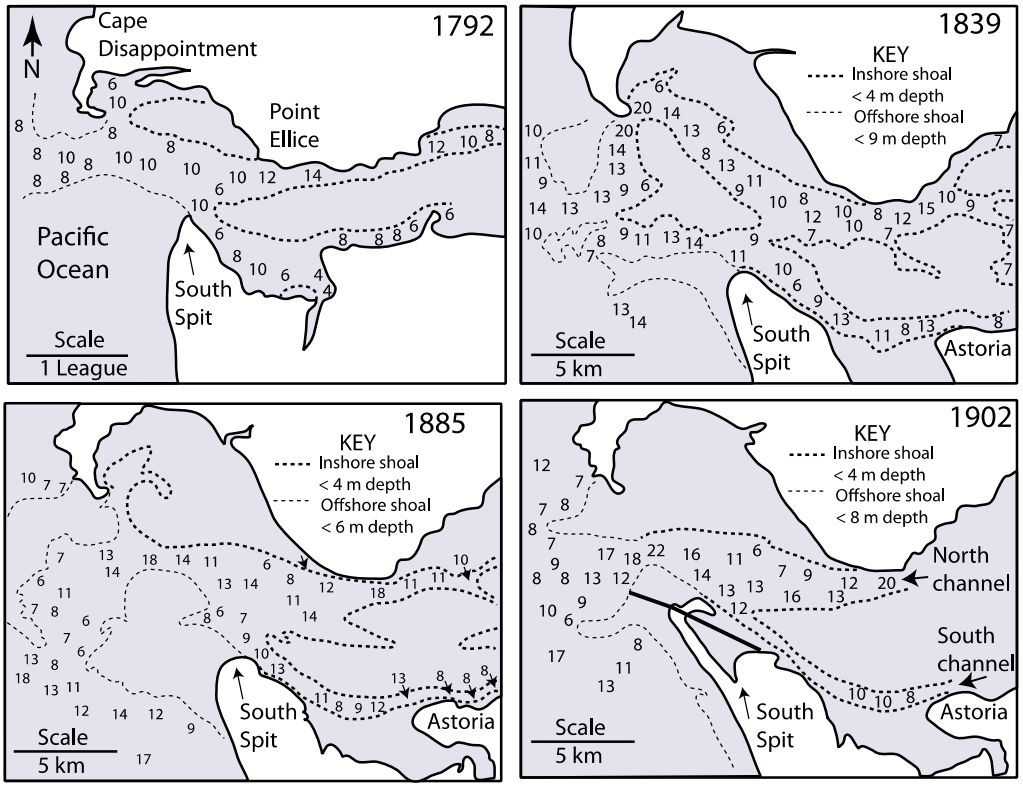

Figure 2. Columbia river mouth geomorphology (1792–1902)

Representative channel depths (m) below sea level and extent of shallow sand shoals including inshore shoals (< 4 m depth) and offshore shoals (< 6, 8 or 9 m depth) are redrafted from Hickson and Rudolf (1951). Jetty construction to stabilize the mouth of the Columbia River at the south spit was initiated (bold line) at the turn of the last century (1902).

Early measurements of riverine–tidal discharge near the Columbia River mouth are presented in Table 1 for representative seasonal conditions of flood and ebb tides (Hickson & Rudolf, 1951). As expected, the early historic river discharges, which existed prior to the numerous impoundments of the Columbia River and its tributaries (Simonstead et al., 1990), exerted a significant asymmetry in tidal flux on a seasonal basis. Combined fluvial–ebb tide discharge exceeded flood tide exchange by 29.7–120.7 percent in the spring months of Columbia River flood. Under maximum river flood conditions, following late–spring snow melt runoff in the eastern tributaries, the fluvial-ebb tide discharge exceeded flood tide discharge by 356 percent. Salt water in the lower estuary generally extends 10–13 km upriver from the mouth in the north and south channels (Figure 2), but it is displaced towards the mouth during spring periods of river flood discharge (CREDDP, 1983). Early historic peak floods (> 35,000 m^3 s^{-1} discharge) have been reduced (< 20,000 m^3 s^{-1} discharge) and shifted into later summer periods by the numerous impoundments (> 130 in number) in the Columbia River tributaries. The impoundments of the Columbia River and its tributaries were constructed after 1937 (Sherwood et al., 1990).

Fox et al. (1984) summarized modern geomorphologic features in the Columbia River estuary to include major and minor tidal channels, and intertidal shoals and marshes. Surface sediments in the Columbia River estuary have been analyzed for grain-size distribution (Sherwood & Creager, 1990). The subtidal flats and deeper

channels are floored by sand. Mud in the modern intertidal deposits is restricted to the protected bays including Baker Bay, Youngs Bay, Grays Bay and Cathlamet Bay (Figure 1). Asymmetric bed forms were imaged on a seasonal basis by side–scan sonar in the estuary during both flood and ebb tidal cycles (Sherwood & Creager, 1990). A predominance of upriver flow orientations demonstrated landward directed salt wedge or gravity flow in the major channel thalwegs (15–20 m depth) in the lowest estuarine reaches. The landward oriented sand waves in the deepest channels (> 15 m water depth) extended 1–13 km upriver of the mouth during fall–winter, but only 1-5 km upriver of the mouth during spring river floods. Seaward–directed asymmetric bed forms dominate the middle reaches of the estuary (13–25 km upriver of the mouth) during all tidal stages throughout the year.

Table 1. Early historic discharge measurements near the mouth of the CRE

Season (1933)	Flood tide length (hr)	Ebb tide length (hr)	Flood tide discharge (m^3 s^{-1})	Ebb tide discharge (m^3 s^{-1})	Discharge difference (m^3 s^{-1})	Discharge difference %
April	5.43	6.90	29367	38090	8723	29.7
May	4.95	7.55	19003	41942	22939	120.7
Max Flood	-	-	-	86800	67797*	356.7
September	5.81	6.44	35598	36985	1387	3.9

Notes: The original data from the mouth of the Columbia River (1933), as provided in cubic feet per second (Hickson and Rudolf, 1951), are converted to cubic meters per second. The total number of tidal cycles averaged for each month in 1933 was April (total 8), May (total 13), and September (total 7). The maximum flood discharge during the May (1933) sampling period is shown under MAX Flood, as reported by Hickson and Rufolf (1951). Percent discharge difference is taken from the ratio of the discharge difference divided by the flood tide and normalized to percent. The maximum flood tide difference is taken from the ratio of maximum discharge difference divided by the May seasonal flood tide discharge and normalized to percent.

Sedimentation rates in the Columbia River estuary during latest Holocene time are established in this study from dated core intervals. Radiocarbon analysis of buried organic materials is supplemented by several methods of relative dating including 1) tephrochonology (Peterson et al., 2012a), 2) cosesimic subsidence (Peterson et al., 2012b), and 3) the first occurrence of introduced mollusks. Four tephra layers of importance to the late Holocene deposits in the estuary were produced by local eruptions from Mount St Helens (Figure 1) including the set-W at 0.5 ka, the set-P at 2.5–3.0 ka and the set-Y at 3.5–4.0 ka, and from an unknown eruptive source (SH/A) at 1.3 ka (Peterson et al., 2012a).

Great earthquakes in the study region (Atwater, 1987; Peterson et al., 2000) have produced episodic events of abrupt submergence (0.5–2.0 m sea level rise) leading to abruptly buried wetland marshes in the Columbia River estuary and adjacent estuaries. Radiocarbon dating has been used to correlate the buried marsh horizons in the lower Columbia River estuary (Jurney, 2001) to regional coseismic susbsidence events (Peterson et al., 2012b). The regional subsidence events include the 1st Sub (AD 1700), 2nd Sub (~ 1.1 ka), 3rd Sub (~ 1.3 ka), 4th Sub (~ 1.7 ka) and 5th Sub (~2.6 ka). Additional microfossil records of these subsidence events in Willapa Bay and Grays Harbor in southwest Washington (Figure 1) coast have been reported by Shennan et al. (1996) and Atwater and Hemphill-Haley (1997).

3. Methods

Continuous cores (7.5 cm diameter) were taken to 4–6 m depth by vibracoring in shallow subtidal shoals, tidal channel accretionary banks, and in fringing tidal marshes (Figure 3). Core sites (58 in number) were selected on the basis of approximately equal distances between stations in across-estuary transects, that were separated at several kilometer distances along the length of the estuary. Major and minor channels were avoided due to historic dredging of the channels for navigation purposes. Early historic bathymetric charts (1839–1902) of the lower reaches (Figure 2) were used to target pre-jetty shoals and muddy tidal flats for vibracoring near the river mouth. Natural intertidal islands and shallow subtidal sand shoals in the middle and upper reaches were selected for vibracoring, based on the earliest triangulated-survey bathymetric charts (1841) of the Columbia River estuary (Wilkes, 1841). Historic bathymetric change maps (CREDDP, 1983) were used to avoid any sites

showing anomalous erosion or accretion, respectively, due to apparent channel dredging and dredge spoil disposal in the estuary.

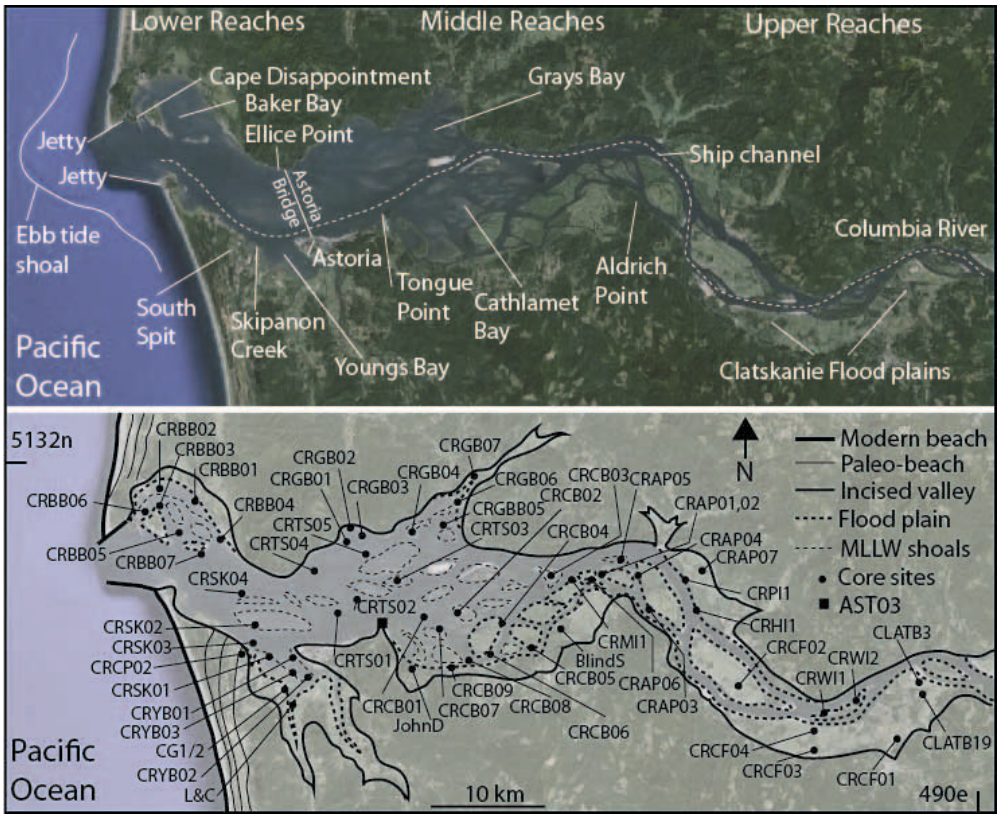

Figure 3. Vibracore sites in Columbia River estuary

Location of core sites (solid black circles) relative to major geographic features (named), intertidal shoals and floodplains (dashed lines) in the Columbia River estuary. Anemometer data is from the AST03 Met Station (solid square) at Tongue Point, 46.208 N 123.767 W (NOAA, 2013). Background imagery is from Google Earth (2013).

Vibracore sites were geo-referenced using GPS-12 channel WASS assisted real time differential processing (+/- 5 m estimated potential error) (Table 2). Core site elevations were estimated on the basis of 1) LiDAR 1/9th arc sec digital elevation models in supratidal and intertidal settings (Pugetsoundlidar, 2013) and 2) measured water depth relative to predicted tide level in subtidal settings. Core site elevations are reported to 0.1 m NAVD88, the reported accuracy of the 1/9th arc sec LiDAR, but are assumed to include vertical errors of +/- 0.25 m due to uncertainties of the horizontal positions (12 channel RT–GPS 2–5 m horizontal error). The regional datum (0 m NAVD88) is about one meter below mean tidal level (MTL). It is nearly equivalent to mean lower water (MLW) in the semidiurnal mesotidal estuary.

The recovered vibracores were split, photographed, and visually logged at the 1.0 cm scale for relative abundances of mud, sand, gravel and peat. Vibracore compression (10–15% length) was corrected proportionally along the full core length, based on the ratio of measured penetration and recovered core length. Core halves were subsampled for 1) average sand size, using an AMCAN™ grain-size card, 2) tephra, and 3) radiocarbon samples. Sand size ranges are as follows: 125–177 µ (fL), 177–250 µ (fU), 250-350 µ (mL), 350–500 µ (mU), 500–710 µ (cL), 710–¡000 µ (cU). The basin bathymetry, wind and wave forcing are used together with deposit grain size to establish sediment transport thresholds that permitted the bypassing of bed load sediments through the estuarine system.

Radiocarbon dating was performed on peat and twig samples to establish basal deposit dates and potential maker bed events, including both tephra layers and buried wetland or subsidence contacts. The radiocarbon samples included 1) wood, as predominantly twigs and small detrital wood fragments mixed with sediments and 2) peat,

as felted roots/leaves in peaty mud layers. Radiocarbon samples were submitted to Beta Analytic Inc., Florida, USA, for AMS radiocarbon dating and age calibration analysis. Some of the radiocarbon dates were previously reported to support the tephrochronology correlation analyses and great earthquake subsidence records in the estuary, as outlined above in Section 2. Target tephra layers in the estuary vibracores, including ash or concentrated lapilli, were confirmed by the presence of isotropic glass shards, as observed in picolyte™ mounting medium under petrographic microcroscopy (250 x). Coseismic subsidence contacts were identified by abrupt upcore decreases in the abundance of peat or densely rooted organic layers.

Table 2. Core site positions and surface elevations in tidal flats and marshes

Core site	UTMe (m)	UTMn (m)	Elev. (m)	Core site	UTMe (m)	UTMn (m)	Elev. (m)
CLATB3	487600	5112700	2.7	CLATB19	487600	5112500	2.1
CRCF01	485650	5111505	3.0	CRWI2	481230	5110120	2.2
CRWI1	478920	5109700	2.0	CRCF03	478128	5106798	3.0
CRCF04	478716	5108806	2.3	CRCF02	471169	5111931	2.9
CRAP07	468292	5122850	2.3	CRHI1	468600	5118980	2.3
CRAP03	463165	5119635	2.8	BlindS	455500	5116700	2.0
CRAP06	457414	5120310	2.5	CRAP02	459790	5120994	1.5
CRAP01	459649	5121591	0.8	CRCB03	453917	5121772	0.7
CRPI1	466140	5122280	2.2	CRAP04	462646	5122022	2.7
CRAP05	461760	5123241	1.9	JohnD	442300	511400	2.0
CRCB09	445714	5113554	1.0	CRCB08	447677	5114436	2.0
CRCB06	449399	5114663	1.1	CRCB05	453548	5115209	0.5
CRCB04	451042	5117507	0.8	CRCB07	445536	5116915	0.9
CRMI1	454240	5119300	2.5	CRCB02	446997	5117868	0.2
CRCB01	444250	5118293	1.0	CRTS01	437319	5119029	0.0
CRTS02	439219	5119871	0.3	CRTS03	443239	5121502	0.9
CRTS05	439294	5123509	0.4	CRTS04	436140	5122544	0.3
CRGB03	438811	5125355	0.4	CRGB01	438024	5124993	0.3
CRGB02	438131	5125626	0.2	CRGB04	443351	5124987	0.9
CRGB05	446032	5125129	0.0	CRGB06	446912	5127269	0.7
CRGB07	445163	5128825	2.5	L&C	433941	5111829	2.0
CG1/2	433408	5111983	2.0	CRYB02	434341	5112676	0.5
CRYB03	433286	5112934	0.1	CRYB01	434369	5113348	0.5
CRCP02	429746	5112576	2.1	CRSK01	431008	5114453	0.0
CRSK03	429214	5115175	0.0	CRSK02	430547	5116771	0.0
CRSK04	429915	5118777	0.1	CRBB07	425106	5123527	0.7
CRBB04	427181	5123970	0.7	CRBB05	423822	5124361	0.4
CRBB06	421631	5126240	0.4	CRBB03	420930	5126481	0.7
CRBB01	424977	5126906	0.7	CRBB02	422668	5128950	0.3

Notes: Core positions are in meters (m) 10N UTM coordinates, easting and northing.

Historic ages of some sand flat deposits were demonstrated by the presence of *Corbicula fluminea* shell fragments, either as articulated valves or in erosional lag layers. *Corbicula* was introduced to the Columbia River

estuary prior to 1937 (Counts, 1985, 1986). The small robust clams (1–3 cm diameter) live on the surface of freshwater sand and gravel deposits. Their presence in core samples indicates deposits of historic age. ^{210}Pb dating of historic core sections in two core sites establish the approximate first occurrence ages of *Corbicula* shells in Grays Bay and Youngs Bay, which are lateral embayments in the estuary (Figure 1) (Petersen et al., 2004). The maximum depths of articulated Corbicula shells in the dated cores corresponded to ^{210}Pb decay curve ages of AD 1910–1920 in the Grays Bay and Youngs Bay tidal flats.

4. Results

Preliminary analyses of modern satellite imagery and deposit surface elevations of the Columbia River estuary (Figure 3; Table 1) indicate three intertidal and supratidal depositional environments including 1) supratidal floodplains (> 2.5 m elevation NAVD88), 2) intertidal marsh islands (~ 1.0–2.5 m elevation), and 3) intertidal sand shoals and channel margins or accretionary banks (1.0 to – 1.0 m elevation). Supratidal floodplains dominate the upper reaches of the estuary. Intertidal marsh islands and sand shoals dominate the middle reaches or central bay region between Tongue Point and Aldrich Point. Intertidal sand shoals and subtidal channels (< – 1.0 m elevation) characterize the central axes of the middle and lower reaches of the estuary. Core sites in the estuary are grouped by geographic areas including in down–river order from east to west 1) Clatskanie floodplains (CRCF), 2) Aldrich Point islands (CRAP), 3) Grays Bay (CRGB), Tongue Point Sands (CRTS), Cathlamet Bay (CRCB), Baker Bay (CRBB), Skipanon Sands (CRSK), and Youngs Bay (CRYB) (Figure 3**).** These geographic areas are briefly characterized by core site surface elevations, dominant sediment grain sizes, and deposit age ranges. Specific islands, sand shoals, and channels in the estuary are individually named elsewhere (USCGS, 1967, 1968).

4.1 Clatskanie Flood Plains

The Clatskanie flood plains represent the constricted upper reaches of the Columbia River estuary. One major deep channel (–10 to –25 m elevation) borders the broad vegetated flood plains (2.1–3.0 m elev.) (Figure 3, Table 2). The relatively shallow flood plain deposits (3–5 depth) are characterized by mud and peaty mud overbank deposits (Figure 4). The flood plain deposits overlie channel accretionary bank deposits of muddy sand or sandy mud, as shown in sties CLATB3, CLATB4, CRWI1, CRWI2 and CRCF02. The muddy sand accretionary bank deposits (at least 2–4 m thickness) overlie channel sand in the medium sand size range, as demonstrated in CRWI1 and CRWI2 and CRCF04. The mud and peaty mud overbank deposits date back to about 2.5–3.0 ka at sites CLATB3, CLATB19, CRCF01 and CRCF04, as based on tephrochronology and basal radiocarbon ages (Table 3).

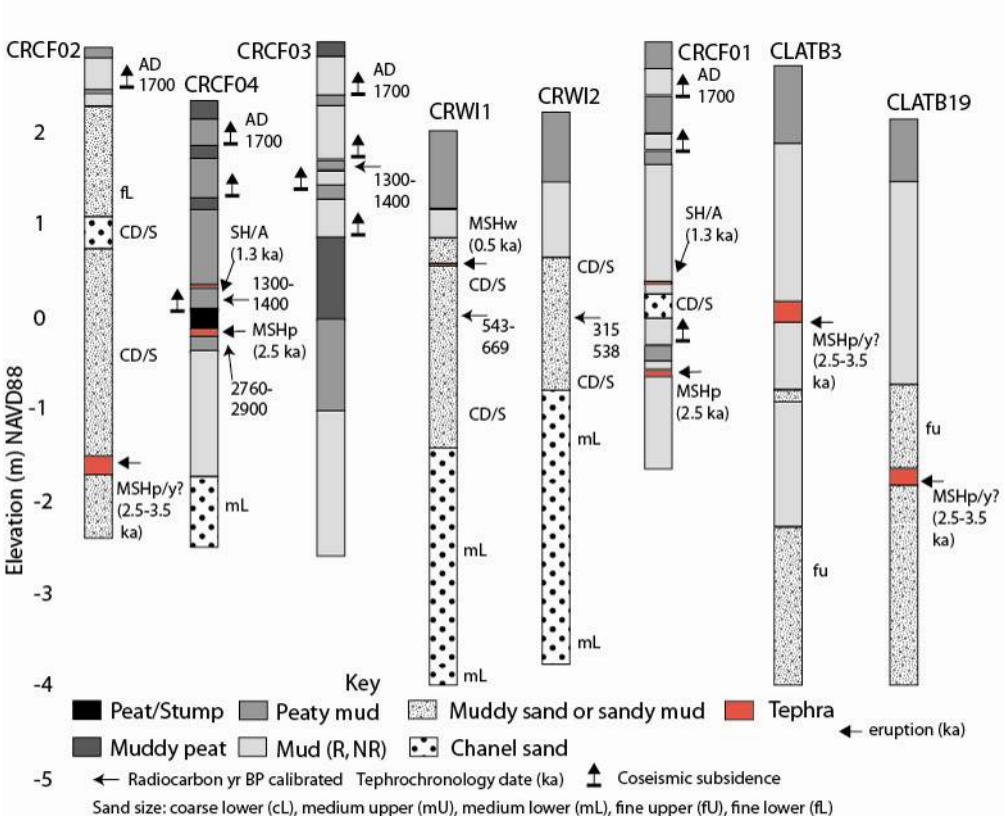

Figure 4. Core logs from vibracores in Clatskanie flood plains

Table 3. Radiocarbon, tephra, subsidence, Pb^{210} and *Corbicula* dates from late holocene tidal flats and marshes

Core site _sample #	Depth (m)	Material	Event age (ka)	Conven- (yr BP)	Calibrated (cal yr BP)	Lab# /Ref
CLATB3	2.70	MSHp/y	2.5-3.5			P(2012a)
CLATB19	3.90	MSHp/y	2.5-3.5			P(2012a)
CRCF01	0.5	1st Sub	0.3			P(2012b)
CRCF01_2.6	2.65	SH/A1.3	1.3			P(2012a)
CRCF01_3.7	3.68	MSHp	2.5			P(2012a)
CRWI2	3.00	organics		420±60	315-538	A(1994)
CRWI1	1.50	MSHw	0.5			P(2012a)
CRWI1	2.00	organics		630±50	543-669	A(1994)
CRCF03	0.65	1st Sub	0.3			P(2012b)
CRCF03_125	1.30	wood		1470±30	1300-1400	B294493
CRCF04	0.5	1st Sub	0.3			P(2012b)
CRCF04	2.0	SH/A1.3	1.3			P(2012a)
CRCF04_205	2.05	wood		1500±40	1310-1510	B294494
CRCF04	2.55	MSHp	2.5			P(2012a)
CRCF04_263	2.63	wood		2730±40	2760-2920	B294495
CRCF02	0.45	1st Sub	0.3			P(2012b)
CRCF02	4.68	MSHp/y	2.5-3.5			P(2012a)
CRAP07	1.35	1st Sub	0.3			P(2012b)

Core site _sample #	Depth (m)	Material	Event age (ka)	Conven- (yr BP)	Calibrated (cal yr BP)	Lab# /Ref
CRAP07_180	1.80	wood		1380±50	1260-1360	B294488
CRAP07	1.85	SH/A1.3	1.3			P(2012a)
CRHI1	0.8	1st Sub	0.3			P(2012b)
CRHI1	1.1	organics		240±60	135-469	A(1994)
CRHI1	1.3	MSHw	0.5			P(2012a)
CRHI1	2.3	organics		780±60	567-900	A(1994)
CRHI1	2.3	organics		880±50	698-916	A(1994)
CRHI1	7.2	organics		1670±70	1397-1732	A(1994)
CRAP03	1.30	1st Sub	0.3			P(2012b)
BlindS	0.6	1st Sub	0.3			P(2012b)
BlindS	0.9	MSHw	0.5			P(2012a)
BlindS	1.1	wood		700±60	552-731	B56407
BlindS	1.3	3rd Sub	1.3			
CRAP06	1.35	1st Sub	0.3			P(2012b)
CRAP02	0.75	1st Sub	0.3			P(2012b)
CRAP01	1.2	MSHw	0.5			
CRAP01	2.5	SH/A	1.3			
CRPI1	0.75	1st Sub	0.3			P(2012b)
CRPI1	0.8	wood		260±50	145-467	CS22498
CRPI1	1.2	MSHw	0.5			P(2012a)
JohnD	0.7	1st Sub	0.3			P(2012b)
JohnD	2.7	5th Sub	2.6			P(2012b)
CRCB08	0.90	1st Sub	0.3			P(2012b)
CRCB05_479	4.79	wood		1230±30	1070-1260	B294492
CRCB09	1.3	*Corbicula*	0.1			
CRMI1	0.7	1st Sub	0.3			P(2012b)
CRMI1	1.2	organics		320±50	296-495	A(1994)
CRMI1	1.5	MSHw	0.5			P(2012a)
CRMI1	2.1	organics		590±50	528-659	A(1994)
CRMI1	4.0	organics		1300±90	989-1368	A(1994)
CRCB02_409	4.09	wood		1210±50	990-1270	B294491
CRCB04	2.9	*Corbicula*	0.1			
CRTS01	2.7	*Corbicula*	0.1			
CRGB06	1.00	Pb210	0.1			P(2003)
CRGB06	4.7	SH/A	1.3			
CRGB07	1.10	1st Sub	0.3			P(2012b)
CRGB04	2.0	*Corbicula*	0.1			
L&C	0.4	1st Sub	0.3		929-1061	J(2001)
L&C	0.7	2nd Sub	1.1		1300-1364	J(2001)
L&C	1.8	3rd Sub	1.3		1300-1364	J(2001)

Core site _sample #	Depth (m)	Material	Event age (ka)	Conven- (yr BP)	Calibrated (cal yr BP)	Lab# /Ref
L&C	2.4	4rd Sub	1.7		1545-1690	J(2001)
L&C	3.3	5th Sub	2.6		2471-2715	J(2001)
CRYB02	0.8	Pb210	0.1			P(2004)
CRYB03	0.7	*Corbicula*	0.1			
CRCP02	0.7	1st Sub				P(2012b)
CRSK02	2.5	*Corbicula*	0.1			
CRBB06	1.5	1st Sub	0.3			P(2012b)
CRBB06	2.7	MSHw	0.5			
CRBB06_528	5.28	wood		1250±30	1080-1270	B294490

Notes: Depth is below floodplain surface level, and does not include artificial fill. Fill depth in MU70 is not known. Wood: predominantly twigs and small detrital wood fragments (wood) and felted roots/leaves in peaty mud (organics). Tephra: predominantly ash size material, except for large lapilli (1 cm) in CRDI sites and lahar in CRSR1 (Peterson et al., 2012a). Tephra dates: MSH set-W (AD 1480), SH/A1.3 ka (1260–1360 BP), MSH set-P (2500–3000 BP), MSH set-Y (3500–4000 BP)(Peterson et al., 2012a). Radiocarbon dates: Beta Analytic Inc., Miami, Florida (B) and Lawrence Livermore Laboratory, Livermore, California (C) are shown as conventional with 1-sigma error and as calibrated with 2-sigma analytical error. Radiocarbon dates are also from Atwater (1994) A (1994). Tephrochronology correlations are from Peterson et al. (2012) P (2012a). The abrupt subsidence contacts (Sub) in L&C are from Jurney (2001) J (2001) and from other core sites are from Peterson et al. 2012b P (2012b). The Pb201 dates in CRGB06 and CRYB02 are from Petersen et al. (2004) P (2004).

4.2 Aldrich Point Islands

The Aldrich Point islands are mid-channel vegetated islands (0.8–2.3 m elevation) that occur in the broadening river valley of the upper-middle reaches of the Columbia River estuary (Figure 3; Table 2). The single major river channel in the upper reaches of the Clatskanie flood plains diverges into 2-4 shallower subtidal channels (5–10 m depth) that surround the Aldrich Point islands. The multiple distributary channels and mid-channel islands in the Aldrich Point area resemble the bay head delta settings of Hill and Fitzgerald (1992) and Dalrymple et al. (1994). The Aldrich Point islands demonstrate shallow peaty mud or mud overbank deposits (0.5–2.0 m depth) above muddy sand accretionary bank deposits or channel sand deposits (Figure 5). The shallow overbank deposits are young, reaching only about 0.5 ka in age in sites CRAPI1, CRAP02, and CRAP03. The older lateral flood plain at BlindS reaches at least 1.3 ka in age based on correlated coseismic subsidence events (3rd Sub at 1.3 ka) (Table 2). The muddy sand accretionary bank deposits (3–5 m thickness) in the Aldrich Point islands demonstrate relatively young ages (0.5–1.3 ka). The oldest channel sand deposit at about 6 m depth or – 3.75 m elevation in CRHI1 yields a basal radiocarbon age of 1.4–1.7 ka. A shallower channel sand deposit at -1.75 m elevation in site CRAP01 is tentatively dated to 1.3 ka by a second thin tephra layer (SH/A at 1.3 ka). The Aldrich Point island deposits (0.5–1.3 ka) are substantially younger than the lateral flood plain deposits (2.5-3.0 ka) in the upper reaches of the Columbia River estuary (Table 3).

4.3 Cathlamet Bay and Grays Bay

The middle reaches of the Columbia River estuary include the two lateral embayments, Calthlamet and Grays Bay, and the intervening intertidal sand shoals (CRTS) in the central axis (Figure 3). Tidal marshes are developed in small tributary head deltas in Cathlamet Bay (JohnD) and Grays Bay (CRGB07) (Figures 6 and 7). Muddy sand deposits in the protected intertidal flats and channel accretionary banks of Cathlamet Bay (CRCB05, CRCB06, CRCB09, CRMI1) and Grays Bay (CRGB06) give way to intertidal sand flats and shallow sand channels (< 10 m depth) in the central axis sand shoals. Muddy sand deposits in channel accretionary banks at –4 to –5 m elevation reach 1.0–1.3 ka in age in Cathlamet Bay (CRCB02 and CRCB05) and Grays Bay (CRGB06). Sedimentation rates in those channel accretionary bank settings reach 3–4 m ka^{-1}. The sedimentation rate for a muddy sand accretionary bank at CRMI (~ 0.5 to –1.5 m elevation) is estimated to be about 3.3 m ka^{-1} for the period from 528–659 to 989–1368. The accretionary bank sedimentation rates are much larger than measured rates of relative sea level rise (~ 0.75 m ka^{-1}) for latest Holocene time in the study area (Peterson et al., 2010). The high sedimentation rates in the accretionary banks might reflect channel cut and fill deposition following

channel lateral migration in middle reaches of the Columbia River estuary. Sedimentation rates of mud and peaty mud in overbank deposits from protected tidal marshes in Cathlamet Bay (JohnD) and Grays Bay (CRGB07) are much lower (1.6–1.8 m ka^{-1}). Those overbank sedimentation rates in the protected tidal marshes more closely follow the relatively low–rates of latest-Holocene sea level rise in the estuary (Peterson et al., 2013).

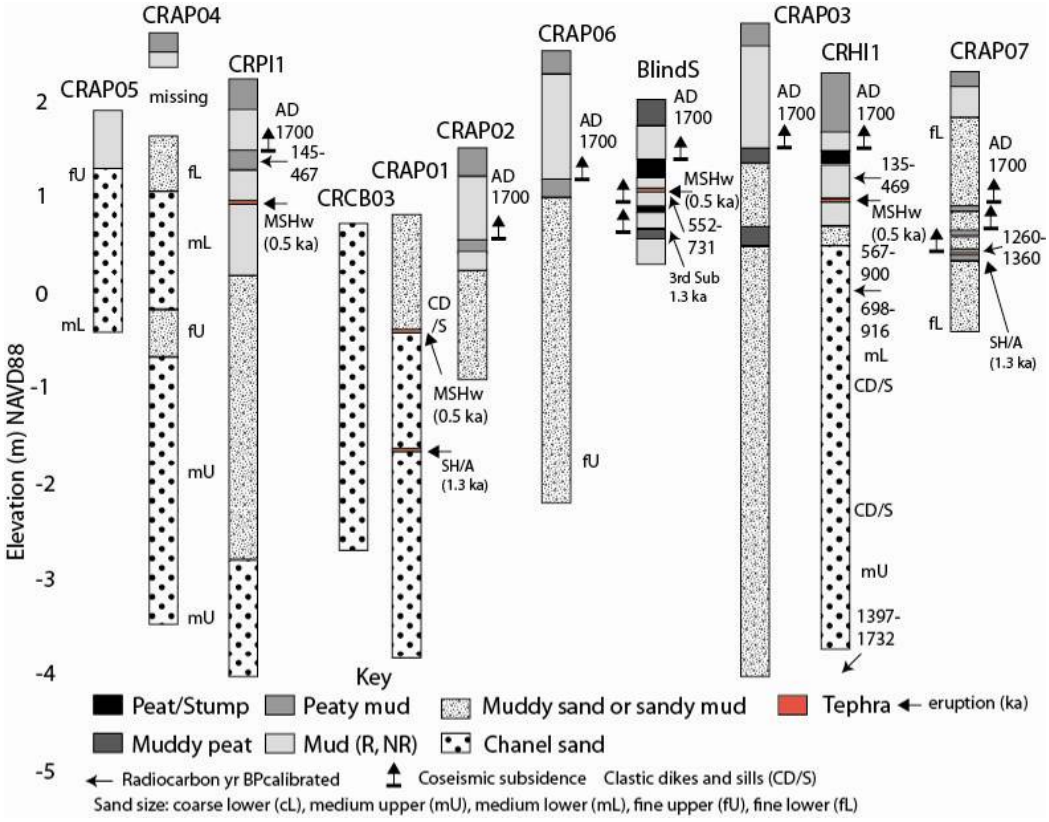

Figure 5. Core logs from vibracores in Aldrich Point islands

4.4 Youngs Bay and Baker Bay

Youngs Bay and Baker Bay are shallow intertidal embayments that are located on either side of the central axis of the lower estuarine reaches, near the mouth of the Columbia River (Figure 3). Youngs Bay and Baker Bay are partially protected from high wave energy entering the mouth of the Columbia River by their leeward positions, respectively behind the south spit and Cape Disappointment. Tidal flats (-1 to 1 m elevation) and marshes (1 to 2 m elevation) have nearly infilled the tidal creek valleys that formed the two embayments (Figure 3; Table 2). Tidal marsh deposits in Youngs Bay (CG1/2 and L&C) record multiple paleotsunami sand sheets (2–4 in number) that are associated with coseismic subsidence events (Sub events # 1–6) at 0.3–2.6 ka (Table 3; Figure 8) (Jurney, 2001). High sedimentation rates (3-5 m ka^{-1}) are found for Baker Bay core sites (CRBB06 and CRBB05) suggesting very rapid infilling of the embayment subtidal flats and/or tidal channel accretionary banks during the last 1,000 years (Figure 9).

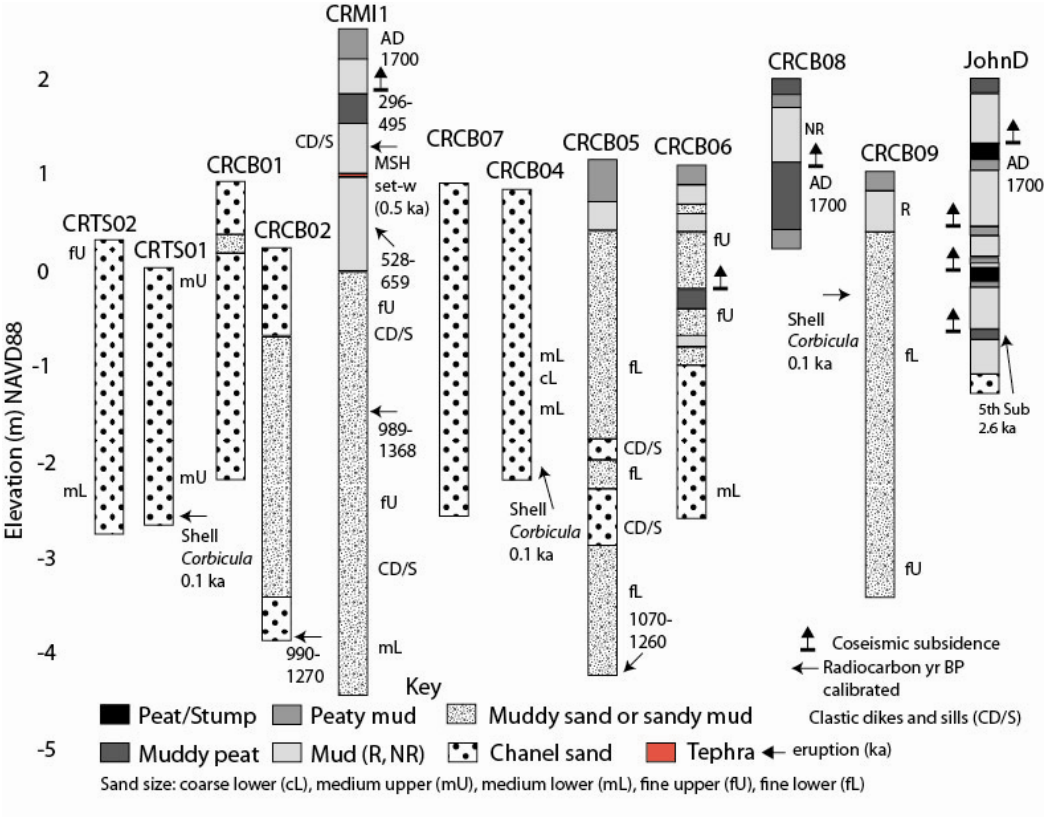

Figure 6. Core logs from vibracores in Cathlamet Bay

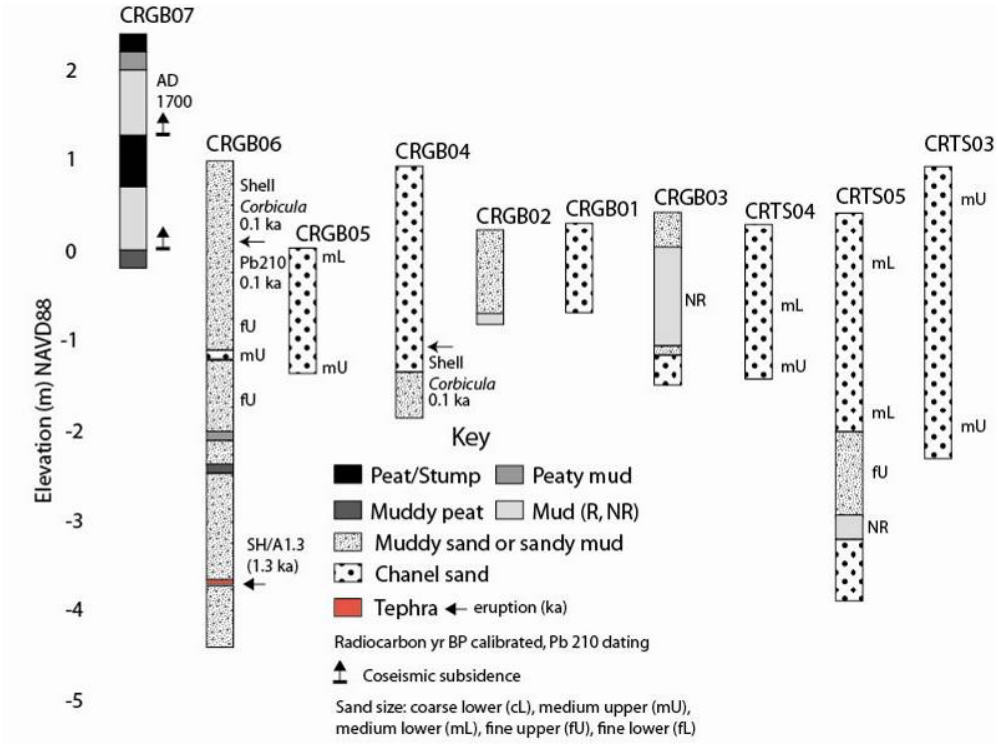

Figure 7. Core logs from vibracores in Grays Bay

4.5 Central Axis Sand Shoals

Muddy sand deposits in the lateral embayments of Cathlamet, Grays, Youngs and Baker Bays (Figure 3) transition to intertidal sand flats and shallow subtidal sand shoals in the central axis regions of the middle reaches (CRTS01, CRTS02, CRTS03, CRTS04, CRTS05, CRCB01, CRCB07) and lower reaches (CRSK03, CRSK02, CRSK04, CRB07) of the estuary (Figures 6, 7, 8, 9). Very–high sedimentation rates are locally indicated for some of the central axis sand shoals, where whole valves or large shell fragments from the *Corbicula* mollusk were found to subsurface depths of more than one meter. *Corbicula* was introduced to the CRE in the early 1900s (Counts, 1985; 1986). The first occurrences of *Corbicula* are locally found to maximum subsurface depths of 2.5 m in site CRSK02, 2.1 m depth in site CRGB04, 2.7 m depth in site CRTS01, and 2.9 m in site CRCB04 (Figures 6, 8, 9).

The historic ages and multi–meter depths of the *Corbicula* shells in some of the central axis sand shoals (Figure 3; Table 3) lead to very–high sedimentation rates of 2–3 cm yr^{-1} in historic time. The very-high sedimentation rates in some of the sand shoals greatly exceed rates of expected relative sea level rise (~ 0.1 cm yr^{-1}) as projected into the last 100 year interval from the latest Holocene sea level curve (Peterson et al., 2010; Peterson et al., 2013). If such high sedimentation rates occurred widely in the central axis of the estuary during latest Holocene time (0 – 2.5 ka) then the shallow subtidal shoals would have converted to intertidal marsh islands and/or to supratidal floodplains prior to historic time. Are such high-sedimentation rates in some of the central axis sand shoals due to 1) anomalous infilling of the lower estuarine reaches following jetty construction or channel dredge spoil disposal (CREDDP, 1983) or 2) natural channel migrations and corresponding cut–and–fill mechanisms in shifting sand shoals? Also, what processes maintained the sand shoals at low intertidal or shallow subtidal levels during historic time and possibly throughout latest Holocene time? These questions are addressed below in the discussion section.

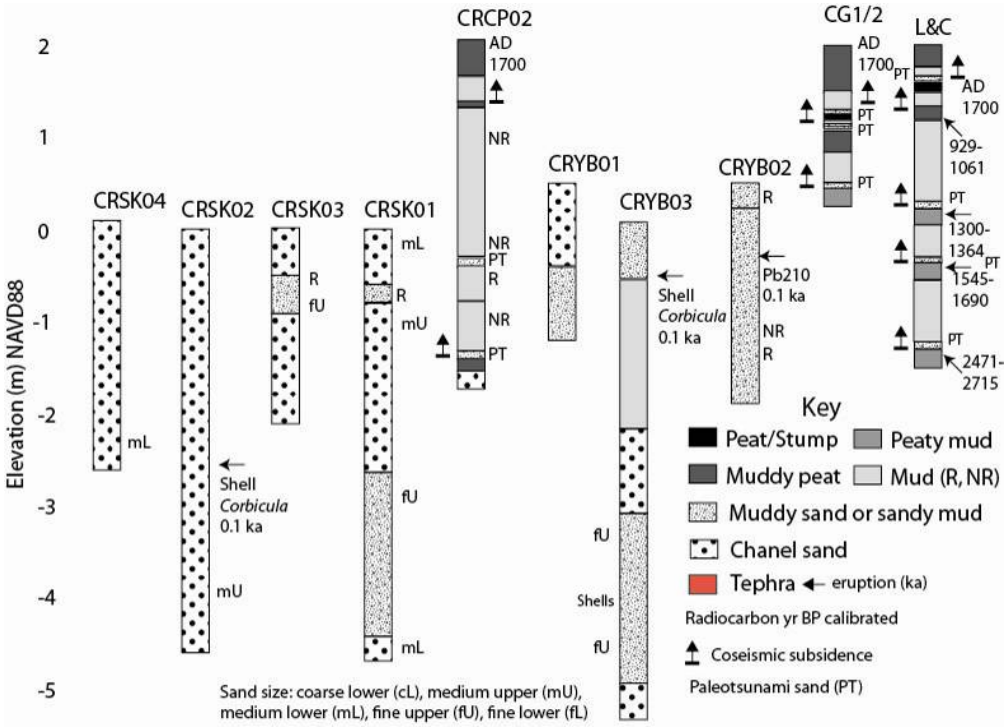

Figure 8. Core logs from vibracores in Baker Bay

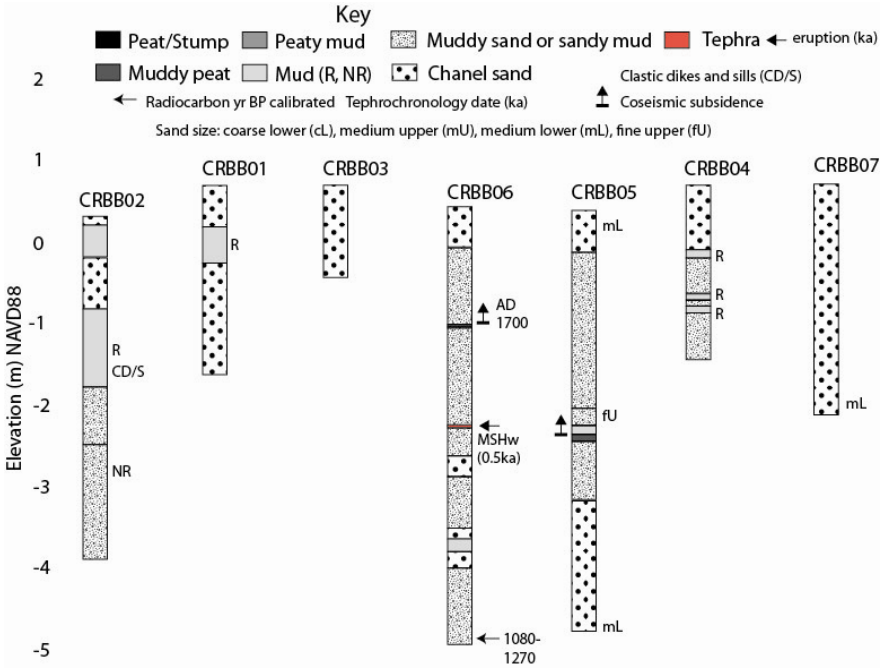

Figure 9. Core logs from vibracores in Youngs Bay

5. Discussion

5.1 Depositional Environments

Core logs from 58 sites in the Columbia River estuary indicate six depositional environments based on dominant sediment textures and cores site elevations (Figure 3). Peaty–mud overbank deposits occur in supratidal floodplains in the upper reaches (Figure 4) and in intertidal marsh islands in the middle reaches (Figure 5). Muddy sand deposits occur in protected lateral embayments and in intertidal accretionary banks in the middle reaches (Figures 5, 6, 7). Sand deposits occur in exposed sand shoals and in subtidal channel deposits in the central axes of the middle and lower reaches (Figures 6–9). Depositional sequences of 1) peaty mud overbank deposits, 2) muddy sand accretionary bank deposits, and 3) sand shoal or sand channel deposits differ substantially in their basal ages (Figures 10A and 11). For example, lateral floodplain progradations in the uppermost reaches of the estuary have constricted the main Columbia River channel(s) to the north of CLATB3 in transect A-A' since 2.5–3.5 ka and between sites CRCF02 and CRCF04, respectively, in transect B–B' since 2.5–3.5 ka and 2.8–2.9 ka. The relative stability of the deep main channel(s) in the uppermost reaches of the estuary contrast with the relative instability of shallow multiple channels in the middle and lower estuarine reaches. Three to four shallow channels separate intertidal marsh islands in transects C–C' and D–D' where muddy accretionary banks (CRAP07, CRAP01, CRMI1, CRGB06, CRCB02, CRCB05) date back to only about1.3 ka at several meters depth subsurface. In the lower estuarine reaches multiple shallow channels (3–4 in number) dissect intertidal sand shoals and shallow subtidal sand shoals in the central axis of the CRE. Sand shoal deposits in transects E–E' and F–F', respectively date from 0.1 ka (CRTS01, CRSK02) to 1.0–1.3 ka (CRCB02), at several meters depth subsurface. The sand shoal basal dates are on the average about five times younger than the floodplain basal dates from similar subsurface depths.

5.2 Geomorphic Controls on Depositional Environments

The older lateral floodplains, dating back to about 2.5 ka, are concentrated in the upper reaches of the Columbia River estuary, especially upriver of Aldrich Point (Figures 3, 11). A narrowing of the Columbia River valley at Aldrich Point (4 km valley width) might have increased the floodwater elevations there, leading to the elevated floodplain surfaces (> 2.5 m elevation) in the uppermost reaches of the estuary. The substantial constriction of the Columbia River valley at Aldrich Point also eliminated the potential for westerly wind–wave erosion in the eastern uppermost reaches of the estuary. The younger intertidal marsh islands and shallow muddy sand flats, dating back to about 1.3 ka, are most prominent in the wider middle reaches (9-14 km in width) of the estuary. Cathlamet Bay is located upriver of Tongue Point on the south shore of the estuary. Grays Bay is located upriver of Point Ellice on the north shore of the estuary. River valley constrictions at Point Ellice and Tongue Point

limited westerly wind-wave propagation into Cathlamet Bay and Grays Bays (Figure 10B).

Protection from wind–wave erosion permitted the development of the intertidal lateral marshes and marsh islands in the protected embayments in the lower and middle reaches of the Columbia River estuary. Cathlamet Bay is particularly well–sheltered from the strongest wind-wave forcing from the southwest (bearings 245-270°) during winter storms (Figure 10B). Only a narrow range of northwest wind-waves from the mouth (bearings 280-285°) can reach the interior of Cathlamet Bay. Grays Bay is sheltered from summer wind-wave forcing from the northwest (bearings 280–310°) and to a lesser extent from southwest wind-waves at bearings less than 240°. Erosional shorelines or gavel lag shorelines presently occur where wind-wave fetch is unobstructed, such as at Point Ellice and Tongue Point (Figure 10B). Intertidal sand shoals and intervening subtidal channels occur in the central axes of the middle and lower reaches. Sand shoals in the middle and lower reaches of the estuary are exposed to wind-waves from both the southwest quadrant (250–270°) and the northwest quadrant (285–310°).

Dated vibracore sequences from the Columbia River estuary do not show expected trends of decreasing sedimentation rates in sites that were most exposed to wind-wave erosion. The sand shoals in the central axes of the lower and middle reaches were exposed to the greatest range in wind–wave bearings and fetch distances in the estuary (Figure 10B). Some core sites in sand shoals in the central axes demonstrate the highest sedimentation rates in the estuary (average 2.5 m per century) (Table 4). These extreme sedimentation rates are recognized by the onset of the introduced *Corbicula* shells at several meters depth in continuous cores. Most core sites in the central axes sand shoals lack Corbicula shells at depth (Figures 5-9), suggesting that the extreme sedimentation rates are highly localized within the central axes areas. Sedimentation rates are also compiled for the marsh islands (average 3.3 m ka^{-1}) and for the tidal flats (average 3.6 m ka^{-1}) in the protected embayments. The modest sedimentation rates in the protected embayments are nearly an order of magnitude smaller than those for localized conditions in the central axes sand shoals. The lateral floodplains in the protected embayments and in the uppermost reaches up–river of Aldrich Point (Figure 4) show the lowest sedimentation rates in the estuary (average 1.1 m ka^{-1}). Some mechanism(s) other than wind-wave erosion must control short–term sedimentation rates in the Columbia River estuary.

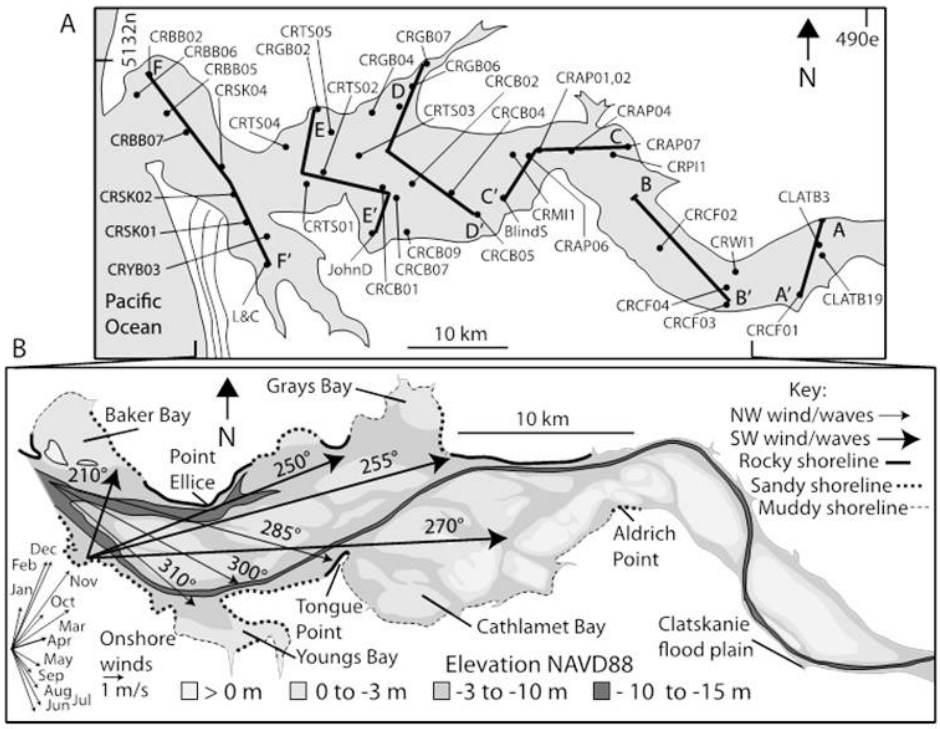

Figure 10. Core site traverses and wind directions

Part A, map of vibracore cross-section traverses and key vibracore sites (numbered). Part B, bathymetry (1968), shoreline types, and westerly wind–wave directions (azimuth in degrees 360° N). Westerly wind–wave fetch distances (arrows) to geographic points in the estuary are shown from the southwest (SW) and northwest (NW)

quadrants. Monthly onshore wind–speeds (arrows in m/s) are from offshore buoy data (Byrnes & Li, 1998). Bathymetry is digitized from 1967 NOAA navigation charts (± 1 ft MLLW converted to m NAVD88) (USCGS, 1967; 1968) that predate the most recent impacts from the Columbia River tributary impoundments and navigation channel deepening.

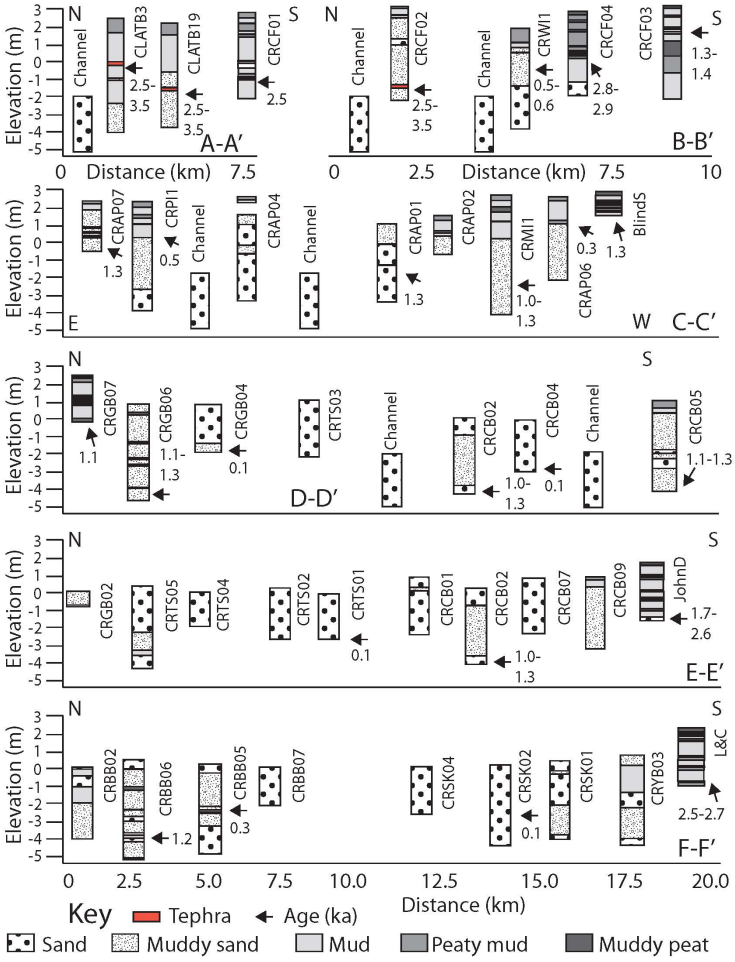

Figure 11. Representative cross sections

Cores site cross-sections in late Holocene floodplains (elevation > 2.5 m), intertidal shoals, accretionary banks, and marshes (0-2.5 m elevation) and subtidal channel deposits (< 0.0 m elevation). See Figure 10A for cross-section traverses

5.3 Sediment Level Curves

Deposit ages versus corresponding elevations (NAVD88) are compared for three sediment types or depositional environments in the Columbia River estuary (Figure 12). Peaty mud represents overbank deposition in floodplains and tidal marshes. Muddy sand represents deposition in intertidal accretionary banks and in protected shallow embayments. Sand represents deposition in intertidal sand shoals and subtidal channel deposits. The floodplain and tidal marsh deposits accumulated overbank mud at 1–2 meters above relative sea level for corresponding ages. Long–term sedimentation rates in the stable floodplains and tidal marshes are controlled by rates of relative sea level rise in the study region (~ 0.75 m ka^{-1}). Rising sea level increases accommodation space in the upper-intertidal and supratidal settings, thereby controlling sedimentation rates of overbank mud deposition. Dated muddy sand and sand deposits generally occur well below sea levels of corresponding age during the last 1,500 years. Their sedimentation rates (1.9–4.2 m ka^{-1}) (Table 4) greatly exceed the corresponding rate of sea level rise (0.75 m ka^{-1}). The rates of sea level rise do not control short-term sedimentation rates in the sand and muddy sand depositional environments of the Columbia River estuary. Instead, the high-sedimentation rates represent short–term cut and fill processes resulting from channel lateral migrations. The very–high

sedimentation rates (> 2.0 m per century) in four core sites from the central axes sand shoals occurred during the middle– to late– historic time of little to no net relative sea–level rise. It is not known whether these anomalous sedimentation rates reflect 1) very recent channel migration events and/or 2) substantially increased sedimentation from anthropogenic impacts, such as impoundment related reductions in peak flood discharge (Jay & Naik, 2011).

Table 4. Sedimentation rates in the CRE vibracore sites

Environment	Core site	Interval depth (m)	Texture	Dates (ka)	Sed. rate (m ka^{-1})
Floodplain					
	CLATB3	0.0-2.7	pm/m	0.0-3.0	0.9
	CLATB19	0.0-3.9	pm/m	0.0-3.0	1.3
	CRCF01	0.0-3.7	pm	0.0-2.5	1.5
	CRCF04	0.0-2.6	pm	0.0-2.8	0.9
	CRCF02	0.0-4.7	sm	0.0-3.0	1.6
	BlindS	0.0-1.3	pm	0.0-1.3	1.0
	JohnD	0.0-2.7	pm	0.0-2.6	1.0
	L&C	0.0-2.4	pm	0.0-2.6	0.9
	average				1.1
Marsh island					
	CRWI2	0.0-3.0	pm/ms	0.0-0.4	7.5
	CRWI1	0.0-2.0	pm/ms	0.0-0.6	3.3
	CRAP07	0.0-1.8	pm/ms	0.0-1.3	1.4
	CRHI1	0.0-2.3	pm/ms/s	0.0-0.7	3.3
	CRAP01	0.0-2.5	ms/s	0.0-1.3	1.9
	CRB05	0.0-4.8	pm/ms	0.0-1.1	4.4
	CRMI1	0.0-3.3	pm/ms	0.0-2.6	1.3
	average				3.3
Protected flat					
	CRAP01	0.0-2.5	ms/s	0.0-1.3	1.9
	CRCB02	0.0-4.1	s/ms	0.0-1.1	3.7
	CRGB06	0.0-4.7	ms	0.0-1.3	3.6
	CRBB06	0.0-5.3	m/s	0.0-1.2	4.2
	average				3.3
Sand shoal					
	CRCB04	0.0-2.9	s	0.0-0.1	29
	CRTS01	0.0-2.7	s	0.0-0.1	27
	CRGB04	0.0-2.0	s	0.0-0.1	20
	CRSK02	0.0-2.5	s	0.0-0.1	25
	average				25

Notes: Depositional environments include 1) mud or peaty mud deposits in laterally accreted floodplains, 2) overbank (mud) and accretionary bank (muddy sand) in intertidal marsh islands, 3) muddy sand in protected intertidal flats, and 4) sand in intertidal shoals and subtidal channel banks. Bounding depth interval (m) is from the surface (0.0 m) to the subsurface depth of the basal date. Deposit grain size facies from top/bottom are as follows: peaty mud (pm), muddy sand or sandy mud (ms), and sand (s). Bounding dates (ka) are taken from the modern surface (0.0) to the basal date at or near the base of the grain size facies sequence. Sedimentation rates (m ka^{-1}) are taken from depth range divided by age range.

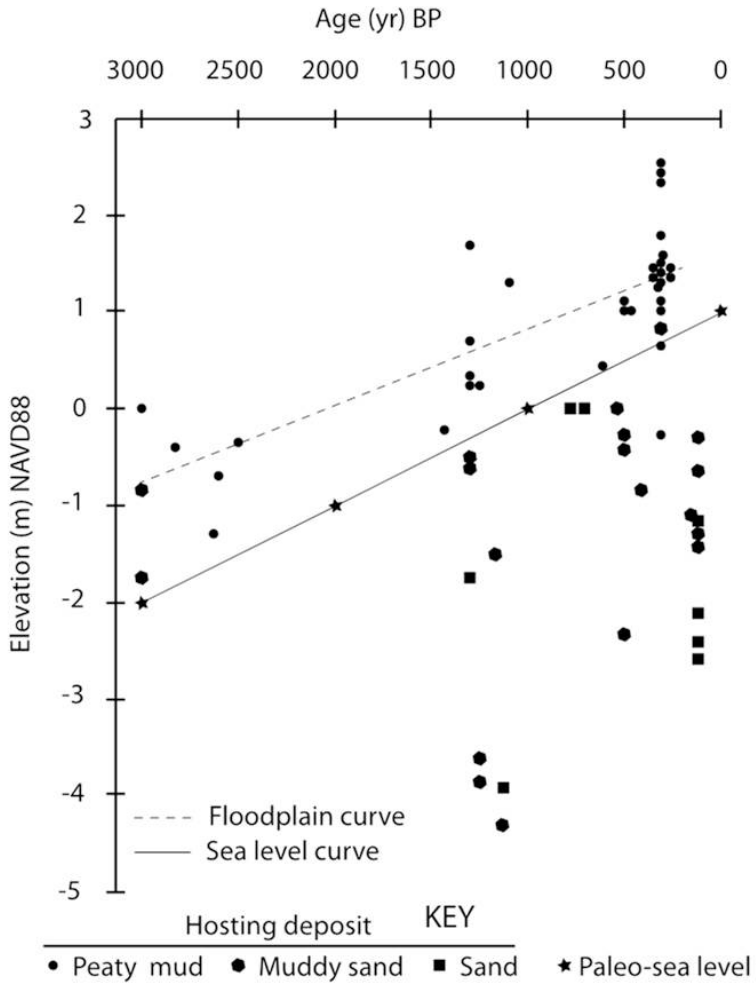

Figure 12. Sediment level and sea level curves

Sediment level curves (deposit age versus elevation) for three depositional settings, as based on 1) peaty mud in supratidal floodplains and upper–interidal marshes (solid circles), 2) muddy sand in protected embayment tidal flats and channel accretionay banks (solid polygons) and 3) sand in channels and shallow sand shoals (solid squares) of the Columbia River estuary. A local relative sea level curve (solid stars) is based on salt marsh data from adjacent tidal bays, Grays Harbor and Willapa Bay (Figure 1) (Peterson et al., 2010). Columbia River estuary data are from Tables 2 and 3.

5.4 Early Historic Bathymetry

Intertidal islands, shallow subtidal shoals, and multiple major tidal channels characterized the early historic bathymetry (1841) of the lower and middle reaches of the Columbia River estuary (Wilkes, 1841). The intertidal islands and shallow subtidal shoals (> -4 m elevation) represented about 80–90 % of the mapped estuary surface area (Figure 13). The major tidal channels (2–3 in number within most cross-sections) ranged from -5 to -20 m in elevation and represented about 10–20 % of the mapped estuary surface area. The 1841 estuary bathymetry differs from the 1968 bathymetry (Figure 10B) in 1) two channels at the pre-jetty river mouth, 2) a wider north channel, and 3) a narrower (pre-dredged) middle channel. In other regards the two plan views of the estuary, separated by more than 100 years in time, show little difference in estuary geomorphology.

Bathymetric profiles (1–6), which were taken along representative track lines in the 1841 bathymetric survey (Figure 13), are shown relative to the NAVD88 datum in Figure 14. The narrow tidal channels in the uppermost middle reaches at profiles 1 and 2 ranged from -5 to -15 m in elevation. The intertidal marsh islands in profiles 1 and 2 represented 50–75% of the cross-section distance. The shallow subtidal shoals (0 to –3 m elevation) represented about 75% of the cross-section distances in profiles 3 and 4 from the widest middle reaches of the estuary. No deep tidal channels (below – 8 m elevation) crossed the middle reaches from west to east at profile 3.

The central axes sand shoals in the lower reaches at profile 5 ranged between 0 and –3 m elevation. The subtidal channels in the lower reaches widened to more than 50% of the cross-section distance in profile 6 at the river mouth. The subtidal sand shoals in the lower and middle reaches of the Columbia River estuary demonstrate a very narrow elevation range (0 to –3 m NAVD88 or 1–4 m below mean tidal level, as taken from lead line soundings (Wilkes, 1841). These relatively uniform elevations of the shallow subtidal sand and muddy sand shoals that existed in early historic time (Figure 14) are attributed to channel bank deposit scalping by wind-wave erosion, as discussed below.

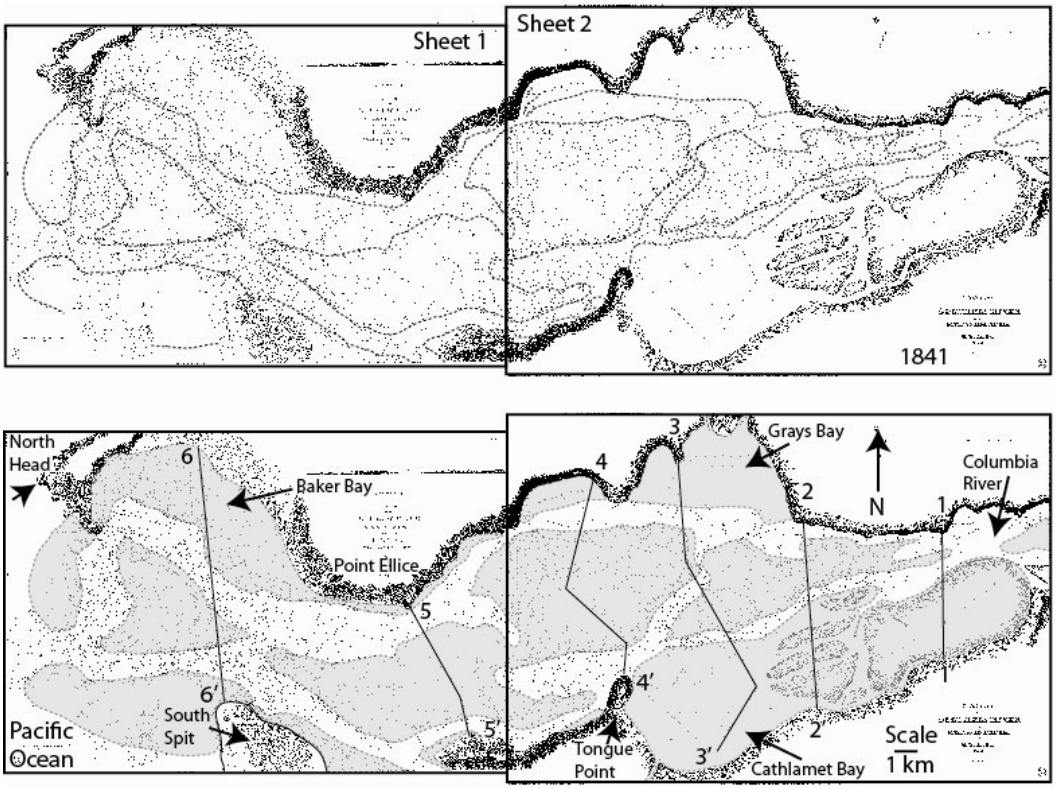

Figure 13. Early bathymetric survey (1841)

Part A: Earliest–historic complete bathymetry (1841) of the Columbia River estuary from the Wilkes Expedition. Small black dots represent soundings on track lines, tied to shoreline navigation points, as surveyed by timed triangulations (Wilkes, 1841). Dotted areas represent shallow shoals, islands, and tidal flats between major tidal channels. Part B: Bathymetry charts (1841) overlain by selected traverses (numbered 1–6) used for bathymetric profiles in Figure 14. Shallow sand shoals (≥ -4 m elev. inshore and ≥ -6 m elev. offshore) are shaded. Marsh islands (above mean sea level) are stippled. Modern geographic features (arrows) are named.

5.5 Wind-Wave Erosion of Shallow Subtidal Sand Shoals

The potential for high wind–wave energy in the Columbia River estuary is provided by coincident river valley enhancements of westerly wind flow and long fetch distances (10–30 km) in the middle and lower reaches (Figure 10B). Wind speed data from the meteorological station AST03 at Tongue Point, OR (Figure 3; NOAA, 2013) are analyzed for the year 2012 to help characterize the potential for wind–wave erosion in the estuary. Wind speeds above 6 m s^{-1} and 8 m s^{-1}, respectively, represent the upper 5 and 2.5 percent of the wind speed interval distribution. Similar wind speed ranges, means and standard deviations are found for the preceding years 2005–2011, as continuously recorded at AST03 (NOAA, 2013). Very–high wind speed periods (average period velocity ≥ 8.0 m s^{-1}) with long durations (period duration ≥ 1.0 hr) are analyzed for date, duration, mean bearing, and mean velocity (Table 5). The longest duration periods (8–21.6 hr) of very–high wind speeds generally occur during the winter season (November to March). They generally blow out of the southwest (bearing 228±43° 1-σ) and typically reach period–averaged velocities of 8–10 m s^{-1}.

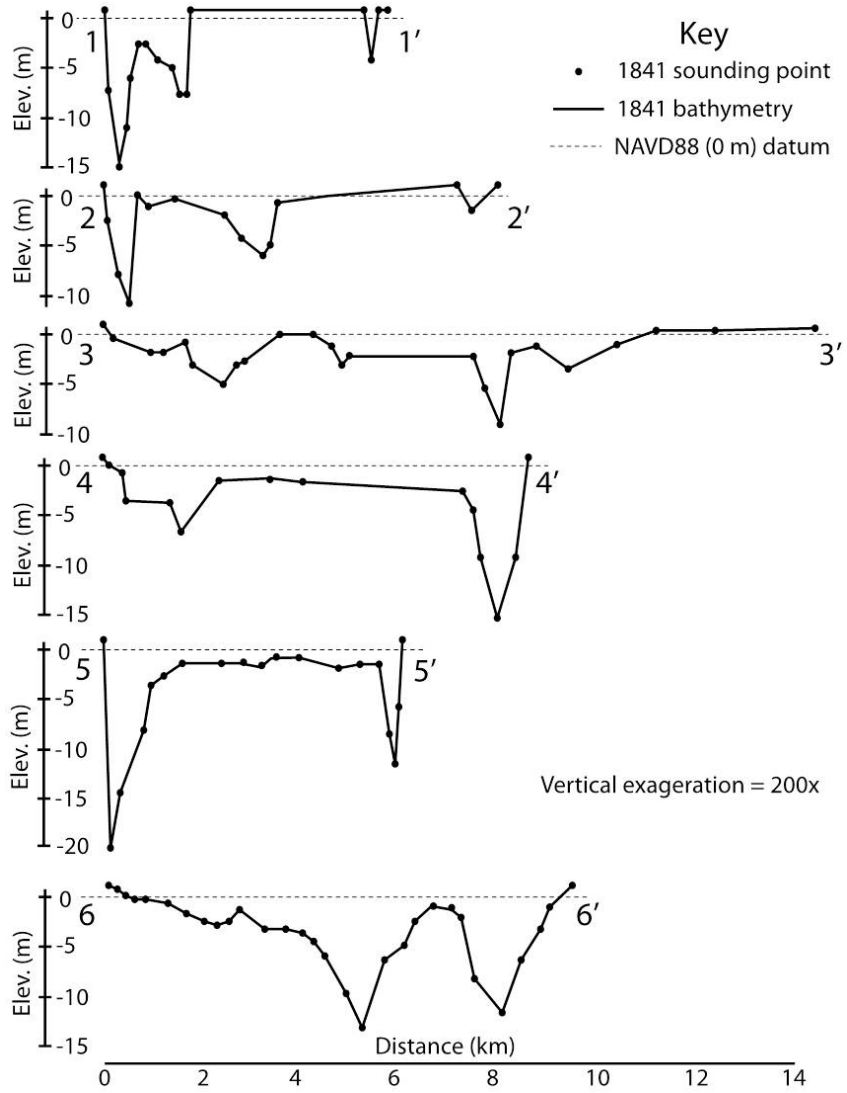

Figure 14. Representative profiles of early bathymetry (1841)

Selected bathymetric profiles from 1841 soundings in the Columbia River estuary. Data are converted to meters (m) NAVD88, assuming mean sea level is at 1.0 m NAVD88.

Table 5. Storm wind-speeds in the Columbia River estuary for the year 2012

Date(s) (yr_mo_dy)	Duration (hr)	Mean wind bearing (°N)	Mean wind velocity ($m\ s^{-1}$)
2012_1_2/3	4.2	206	10
2012_1_5	4.3	211	9
2012_1_14	1.2	289	8.0
2012_1_14	3.0	275	9
2012_1_19	7.0	214	9
2012_1_21	1.3	194	8
2012_1_21	1.0	201	11
2012_1_25	8.8	209	10
2012_1_25	2.2	214	9
2012_1_26	2.4	203	9
2012_2_18	1.6	228	9

2012_2_18	1.4	238	9
2012_2_18	9.9	249	9
2012_2_22	21.6	223	9
2012_2_25	17.5	288	11
2012_2_29	1.9	252	8
2012_3_6	1.2	317	9
2012_3_9	1.0	228	9
2012_3_15	6.6	190	10
2012_3_15	4.8	202	9
2012_3_20	1.4	204	9
2012_3_25	1.8	223	9
2012_3_28	1.0	203	9
2012_3_29	2.1	190	8
2012_3_29	1.5	203	10
2012_5_23	6.9	214	9
2012_7_24	1.0	346	8
2012_8_23	1.0	342	8
2012_8_25	1.4	347	9
2012_8_31	1.0	347	8
2012_9_6	4.1	238	8
2012_9_12	5.4	328	9
2012_10_2	1.1	350	8
2012_10_14	1.0	197	9
2012_10_16	8.4	193	9
2012_10_19	1.4	198	8
2012_10_28	5.9	210	9
2012_11_12	9.2	201	8
2012_11_12	1.0	204	9
2012_11_19	9.2	191	12
2012_11_30	3.4	205	9
2012_11_30	1.9	194	8
2012_12_2	4.2	207	8
2012_12_4	3.6	210	9
2012_12_17	3.1	206	9
2012_12_17	4.4	210	11

Notes: Maximum storm–wind dates (year-month-day), duration (hours), average bearing (degrees North) and velocity (meters per second) are compiled for very-high wind speed periods (grouped wind speed intervals ≥8 m s^{-1}) of at least 1.0 hour duration. The anemometer–recorded wind speeds are averaged over short 0.1 hr intervals, totaling 87,501 intervals for the year. Interval wind speeds ranged from 0.1 to 17 m s^{-1} and yielded relatively low mean velocities (2.6±1-σ 2.0 m s^{-1}). Maximum storm-wind periods were taken at significant increases of interval speed (onset speed ≥ 8.0 m $^{-1}$) and decreases of interval speed (termination speed < 8.0 m $^{-1}$). Wind speed interval data (intervals = 0.1 hr duration) were collected consecutively for the year 2012 (87,501 intervals) at the AST03 Station (anemometer 6.7 m height) located at Tongue Point, OR (46.208°N 123.767°W; Figure 3) by the US National Data Buoy Center (NOAA, 2013).

Wind–wave developments during the very–high wind speed periods (assumed 8 m s^{-1} and 10 m s^{-1}) (Table 5) are estimated for fetch distances of 10, 20 and 30 km and limiting water depths of 1–4 m over the shallow sand shoals (Figure 14; Table 6). These approximations are based on linear wave theory using the SPMWave.html calculator (USGS, 2013a) for the short–period wind–waves. The estimated wind-waves that develop in these conditions range from 0.2 to 0.7 m in wave height. The corresponding near-bottom wave orbital velocities are estimated for representative water depths of 1.0-4.0 m depth (Table 7), using the RunWaveCalcs.html calculator (USGS, 2013b). The threshold of sand shoal erosion is estimated to occur at near–bottom orbital velocities > 0.2 m s^{-1} (Hjulström, 1939; Sundborg, 1956) corresponding to maximum water depths of 1.0–3.0 m, for the wave

heights of 0.3–0.6 m. The shallow depths of sand resuspension by wind–wave orbital motions are consistent with the elevations of the shallow subtidal sand shoals (0 to -3 m NAVD88) in the central axes of the middle and lower reaches (Figure 14). The broad bimodal distribution of high wind–speed bearings, ranging from 190° to 350° (Table 5), likely accounts for the infrequent wind-wave resuspension of muddy-sand in the shallow bottoms of the lateral embayments such as in Grays Bay, Youngs Bay, and Grays Bay (Figures 10B and 11).

Table 6. Predicted wind–wave height and period

Wind Speed ($m\ s^{-1}$)	Fetch Distance (km)	Water depth (1.0 m) Wave ht (m)/ period (s)	Water depth (2.0 m) Wave ht (m)/ period (s)	Water depth (3.0 m) Wave ht (m)/ period (s)	Water depth (4.0 m) Wave ht (m)/ period (s)
8.0	10	0.24/2.0	0.34/2.2	0.39/2.4	0.41/2.4
	20	0.25/2.2	0.39/2.5	0.47/2.2	0.52/2.8
	30	0.26/2.3	0.41/2.7	0.51/2.9	0.58/3.0
10.0	10	0.3/2.2	0.4/2.5	0.5/2.6	0.52/2.6
	20	0.3/2.4	0.5/2.8	0.6/3.0	0.65/3.1
	30	0.3/2.5	0.5/2.9	0.6/3.2	0.71/3.3

Notes: wind–wave height (m) and period (s) are predicted on the basis of wind speed (8 and 10 ms^{-1}), fetch distance (km), and water depth (m), using SPMWave.html calculator (USGS, 2013a). Wave development is not duration limited for long periods (multiple hours) of very-high wind velocity over fetch distances (10–30 km) in the Columbia River estuary (Figure 10b). Assumed water depths are based on bathymetric profiles over intertidal and shallow subtidal sand shoals (> -4 m elevation) surveyed in 1841 (Wilkes, 1841).

5.6 Conceptual Models of Sand Deposition, Re–Suspension, and Throughput in the Central Axes

The Columbia River estuary was supplied with abundant sand (> 5 million $m^3\ yr^{-1}$) during late Holocene time (Peterson et al., 2013), but the estuary failed to infill with upper-intertidal overbank deposits. Measured sedimentation rates in the central channel axes and lateral embayments (Table 4) were substantially greater than coeval rates of sea level rise (Figure 12). The high sedimentation rates resulted from tidal channel lateral migration and corresponding cut–and–fill deposition (Figure 15). Given the high-sedimentation rates in the estuary it would be expected that overbank deposition would have followed the channel cut and fill sequences. Instead, shallow sand shoals (0 to –4 m elevation) dominated the central axes in the middle and lower reaches (Figures 13 and 14) (Wilkes, 1841). The central axes sand deposits were eroded by wind-waves (Tables 5–7) that developed under conditions of long fetch distances (Figure 10B) and winter periods of westerly storm winds. The maximum storm wind velocities (8–10 $m\ s^{-1}$) and long fetch distances (20–30 km) are estimated to have yielded near–bottom orbital velocities of greater than 0.2 $m\ s^{-1}$ at water depths of 2–3 m. Superimposed on the 3.0 m tidal range in the estuary the maximum wind-wave erosion of the central axes sand shoals could have extended downward to 4 m below mean tidal level or -3 m NAVD88.

Wind-wave resuspensions of sand and muddy sand deposits in the exposed shallow shoals (Figures 10B and 11) were superimposed on tidal flood and ebb currents in the mesotidal estuary. Tidal currents are assumed to have drifted the wind–wave resuspended sediments to tidal channels, where combined riverine and tidal ebb flows then transported the sediments seaward (Figure 16). There is a potential seasonal offset between maximum wind-wave erosion in winter (Table 5) and maximum river discharge in spring (Table 1) in the Columbia River estuary. Sand that was stripped from the shallow shoals and delivered to deeper shoal margins and tidal channels in winter (November–March) was subsequently transported seaward by asymmetric riverine–tidal flow during prolonged spring floods (April–June) (Sherwood et al., 1990; Jay & Naik, 2011; Jay et al., 2011). The seaward transport of bed load occurred in shallow tidal channels (> -10 m NAVD88) and in the subtidal sand shoals (–1 to –4 m elevation) (Figure 13). These seaward–transport corridors are located well above the strongest gravity–driven flows in the partially stratified deep channels (-10 to -20 m elevation) near the tidal inlet (CREDDP, 1983; Jay & Smith, 1990). Small inflows of bed load in the bottoms of the deepest tidal inlet channels were outmatched by much greater outflows of bed load across the shallow tidal channel margins and subtidal shoals in the lower estuary reaches.

Table 7. Estimated near–bottom orbital velocities from predicted wind–waves and water depths

Wave height (m)	Wave period (s)	Water depth (m)	Orbital velocity (m s-1)
0.2*	2.0	1.0	0.20
		2.0	0.08
		3.0	0.03
		4.0	0.01
0.3#	2.2	1.0	0.34
		2.0	0.15
		3.0	0.07
		4.0	0.03
0.4*	2.7	1.0	0.51
		2.0	0.28
		3.0	0.17
		4.0	0.10
0.5#	2.8	1.0	0.65
		2.0	0.36
		3.0	0.22
		4.0	0.14
0.6#	3.2	1.0	0.81
		2.0	0.45
		3.0	0.33
		4.0	0.22
0.7#	3.3	1.0	0.96
		2.0	0.58
		3.0	0.39
		4.0	0.28

Notes: wind–wave orbital velocity (m s^{-1}) is estimated for predicted wave height (m), wave period (s), and water depth (Table 6), using RunWaveCalcs.html calculator (USGS, 2013b). Representative wave parameters are from predicted wind speeds of 8.0 m s^{-1} (*) and 10 m s^{-1} (#). Orbital velocities > 0.2 m s^{-1} are above the threshold for sand erosion.

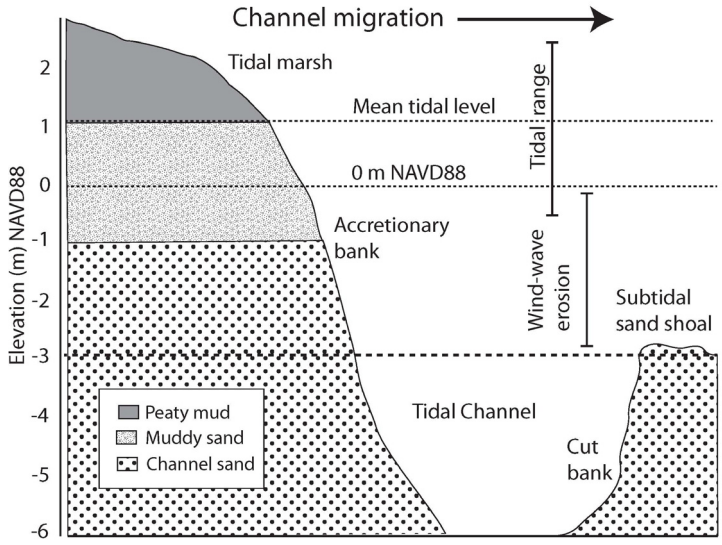

Figure 15. Hypothetical cross–section showing wind–wave erosion

Cross-section diagram of tidal channel, accretionary bank, and subtidal sand shoal environments in the Columbia River estuary. Representative elevations are taken from vibracore sites (Table 2) and early historic bathymetric surveys (Figure 14). Maximum depth of wind-wave erosion (-3 m elevation NAVD88) is based on estimated maximums of wind-wave heights (Table 6) and corresponding near–bottom wave orbital velocities > 0.2 m s^{-1} at 0–4 m water depth or > -3 m NAVD88 (Table 7).

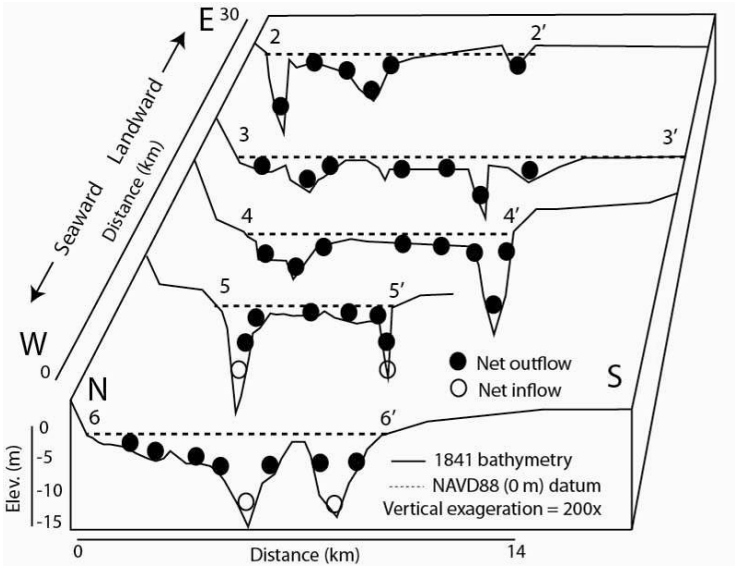

Figure 16. Hypothetical directions of annual net flow

Diagram of middle and lower reaches of the Columbia River estuary showing major tidal channel and subtidal shoal bathymetries from across-estuary profiles (2–6) taken in 1841 (Figure 14). Landward bed form orientations (open circles) indicate net bed load inflow in the deepest channels (< -15 m NAVD88) of the lowest estuary reaches (Sherwood and Creager, 1990). Net seaward flows dominate the middle estuary reaches (solid circles) and the shallow water depths (>–10 m NAVD88) in the lower reaches, particularly during spring river flooding (Table 1). The overall asymmetry of riverine-tidal advection in the shallow tidal channels and subtidal shoals transports sand through the central axes of the estuary to the Pacific Ocean.

6. Conclusions

Traditional models of incised valley accommodation space (Dalrymple et al., 1994; Heap & Nichol, 1997; Smith et al., 2009) do not explain the paradox of abundant bed load supply and an unfilled central bay in the large Columbia River estuary. The paradox in the Columbia River estuary is resolved by analyzing prehistoric core deposits, early historic bathymetry and riverine-tidal discharges, and modern wind-wave forcing conditions. Sediment grain size and deposit age relations are derived from dated vibracore sequences. These data provided sedimentation rates for representative depositional settings during the latest Holocene (0–2,500 ^{14}CyrBP). Low sedimentation rates for peaty mud deposits in semi-stable floodplain and marsh island settings were controlled by low rates of net sea level rise in the estuary. In contrast, high sedimentation rates in muddy sand accretionary banks and in sandy channel deposits exceeded coeval rates of sea level rise. High sedimentation rates in the sand and muddy sand deposits in the central axes and in some lateral embayments of the estuary were related to relatively high rates of recent channel lateral migration. The oldest sand deposits that were preserved at several meters depth in the middle and lower estuary reaches extend back to only 1,500 yeas in age. The high sedimentation rates should have led to central bay infilling by overbank mud deposition in upper–intertidal marsh islands and/or lateral floodplains. However, near–bottom orbital velocities of the large wind–waves eroded the sand shoals to shallow subtidal depths during major winter storms. The seasonal erosion of channel accretionary banks by winter wind–waves prevented the central bay from infilling with overbank mud deposits. The remobilized bed load sediments were delivered to deeper shoal margins and tidal channels in winter months. During subsequent spring months of river flooding (Jay et al., 1990; Jay & Naik, 2011; Jay et al., 2011) the strong asymmetries in riverine-tidal discharges in the shallow shoals and tidal channels transported sand seaward to the Pacific Ocean. These unusual circumstances permitted the shallow Columbia River estuary to bypass bed load to the marine side (Gates, 1994; Baker et al., 2010, Peterson et al., 2013) and yet to remain unfilled by upper–intertidal overbank deposits in the central axes and in the larger lateral embayments for the last several thousands of years.

Acknowledgements

Diana Baker, Dave Qualman, Jeff Heeren and Rebecca Treat assisted with vibracoring and core logging. David Percy provided core site elevations from LiDAR digital elevation data. The USGS (USGS Coop. Agreement #1434-HQ-96-AG-01612) provided support for field logistics. Lethbridge College, Alberta, Canada, provided the support for radiocarbon dating of the Columbia River estuary deposits.

References

Atwater, B. F. (1987). Evidence for great Holocene earthquakes along the outer coast of Washington State. *Science, 236*(4804), 942-944. http://dx.doi.org/10.1126/science.236.4804.942

Atwater, B. F., & Hemphill-Haley, E. (1997). Recurrence intervals for great earthquakes of the past 3,500 years at northeastern Willapa Bay, Washington. *US Geological Survey Professional Paper,* (1576), 1-108.

Baker, D., Peterson, C., Hemphill-Haley, E., & Twichel, D. (2010). Holocene Sedimentation in the Columbia River Estuary. *Marine Geology, 273*, 83-95. http://dx.doi.org/10.1016/j.margeo.2010.02.005

Boyd, R., Dalrymple, R. W., & Zaitlin, B. A. (Eds.). (1994). *Incised-valley systems: origin and sedimentary sequences*. SEPM (Society for Sedimentary Geology).

Byrnes, M. R., & Li, F. (1998). *Regional analysis of sediment transport and dredged material dispersal patters, Columbia River mouth, Washington/Oregon* (pp. 53). Final Report to US Army Corps of Engineers Waterways Experiment Station. Applied Coastal Research and Engineering, Inc. Mashpee, MA.

Counts III, C. L. (1986). The zoogeography and history of the invasion of the United States by Corbicula fluminea(Bivalvia: Corbiculidae). *American Malacological Bulletin, 1986.*

Counts, C. L. III. (1985). Corbicula fluminea (Bivalvia: Corbiculidae) in the state of Washington in 1937, and in Utah in 1975. *Nautilus, 99*, 18-19.

CREDDP. (1983). *Columbia River Estuary Data Development Program* (p. 16). Bathymetric Atlas of the Columbia River. Astoria, Oregon.

Fox, D. S., Bell, S., Nehlsen, W., & Damron, L. (1984). *The Columbia River Estuary: atlas of physical and biological characteristics* (p. 87). Columbia River Data Development Program. Astoria, Oregon.

Gates, E. B. (1994). *The Holocene sedimentary framework of the lower Columbia River basin* (Master's thesis). Portland State University.

Gelfenbaum, G., & Kaminsky, G. M. (2010). Large-scale coastal change in the Columbia River littoral cell: An overview. *Marine Geology, 273*, 1-10. http://dx.doi.org/10.1016/j.margeo.2010.02.007

Google Earth. (2013). Google Earth 2013. Data from SIO, NOAA, U. S. Navy, NGA, GEBCO, Landsat. Retrieved from http://www.google.com/earth/

Heap, A. D., & Nichol, S. L. (1997). The influence of limited accommodation space on the stratigraphy of an incised–valley succession: Weiti River estuary, New Zealand. *Marine Geology, 144*, 229-252. http://dx.doi.org/10.1016/S0025-3227(97)00107-2

Hickson, R. E., & Rodolf, F. W. (1951). History of Columbia River jetties. Proceedings of the First Conference on Coastal Engineering. Coastal Engineering, Chapter 32, pp. 283-298.

Hill, M. C., & Fitzgerald, D. M. (1992). *Evolution and Holocene stratigraphy of Plymouth, Kingston, and Duxbury Bays, Massachusetts*. Quaternary Coastal Systems of the United States, Marine and Lacustrine Systems, SEPM Special Publication No. 48, pp. 45-56.

Hjulström, F. (1939). Transportation of Debris by Moving Water. In P. D. Trask (Ed.), *Recent Marine Sediments*. A Symposium. *American Association of Petroleum Geologists*. pp. 5-31.

Jay, D. A., & Naik, P. (2011). Distinguishing human and climate influences on hydrological disturbance processes in the Columbia River, USA. *Hydrological Sciences Journal, 56*, 1186-1209. http://dx.doi.org/10.1080/02626667.2011.604324

Jay, D. A., & Smith, J. D. (1990). Circulation, density structure, and neap–spring transitions in the Columbia River estuary. *Progress in Oceanography, 25*, 81-112. http://dx.doi.org/10.1016/0079-6611(90)90004-L

Jay, D. A., Giese, B., & Sherwood, C. R. (1990). Energetics and sedimentary processes. *Progress in Oceanography, 25*, 157-174. http://dx.doi.org/10.1016/0079-6611(90)90006-N

Jay, D. A., Leffler, K., & Degens, S. (2010). Long-term evolution of Columbia River tides. *Journal of Waterway, Port, Coastal,and Ocean Engineering, 137*(4), 182-191. http://dx.doi.org/10.1061/(ASCE)WW.1943-5460.0000082

Jurney, C. (2001). *Refining the measured frequency of great earthquakes along the Cascadia subduction zone* (Master's thesis), Central Washington University, Ellensberg.

NOAA. (2013). *National Data Buoy Center, Station AST03-9439040, Astoria, OR. National Oceanic and Atmospheric Administration*. Retrieved December 21, 2013, from http://ndbc-load.nws.noaa.gov/station_history.php?station=asto3

Petersen, J., Reisenbichler, R., Gelfenbaum, G., Peterson, C., Baker, D., Leavitt, P., … Prahl, F. (2004). *Historical changes in the Columbia River estuary based on sediment cores: feasibility studies*. U.S. Geological Survey, Open-File Report.

Peterson, C. D., Cruikshank, K. M., & Darienzo, M. E. (2012b). Coastal tectonic strain and paleoseismicity in the South Central Cascadia Margin, Oregon, USA. In K. Konstantinou (Ed.), *Natural Disaster Research, Prediction and Mitigation: Earthquakes: Triggers, Environmental Impact and Potential Hazards*. NOVA Open Access Publisher, New York. Chapter 1, pp. 1-37.

Peterson, C. D., Doyle, D. L., & Barnett, E. T. (2000). Coastal flooding and beach retreat from coseismic subsidence in the central Cascadia margin, USA. *Environmental and Engineering Geology, 6*, 255-269.

Peterson, C. D., Gates, E. B., Minor, R., & Baker, D. L. (2013). Accommodation space controls on the latest Pleistocene and Holocene (16-0 ka) sediment size and bypassing in the Lower Columbia River Valley: A large fluvial-tidal systems in Oregon and Washington, USA. *Journal of Coastal Research, 29*, 1191-1211. http://dx.doi.org/10.2112/JCOASTRES-D-12-00172.1

Peterson, C. D., Minor, R., Gates, E. B., Vanderburgh, S., & Carlisle, K. (2012a). Correlation of Tephra Marker Beds In Latest Pleistocene and Holocene Fill Of The Submerged Lower Columbia River Valley, Washington and Oregon, U.S.A. *Journal of Coastal Research, 28*, 1362-1380. http://dx.doi.org/10.2112/JCOASTRES-D-11-00181.1

Peterson, C. D., Roberts, M. C., Vanderburg, S., Minor, R., & Percy, D., (2014). Late Holocene chronology and geomorphic development of fluvial-tidal floodplains in the upper reaches of the lower Columbia River valley, Washington and Oregon, USA. *Geomorphology, 204*, 123-135. http://dx.doi.org/10.1016/j.geomorph.2013.07.033

Peterson, C. D., Vanderburgh, S., Roberts, M. C., Jol, H. M., Phipps, J. P., & Twichell, D. C. (2010). Composition, age, and depositional rates of Holocene shoreface deposits under barriers and beach plains of the Columbia River littoral cell, USA. *Marine Geology, 273*, 62-82. http://dx.doi.org/10.1016/j.margeo.2010.02.004

Pugetsoundlidar. (2013). *Columbia River 2005-Lidar Metadata*. Retrieved February 26, 2013, from http://pugetsoundlidar.ess.washington.edu/lidardata/metadata/pslc2005Columbia/columbia05_ascii.html

Shennan, I., Long, A. J., Rutherford, M. M., Green, F. M., Innes, J. B., Lloyd, J. M., … Walker, K. J. (1996). Tidal Marsh stratigraphy, sea-level change and large earthquakes, I: a 5000 year record of large earthquakes in Washington, USA. *Quaternary Science Reviews, 15*, 1023-1059. http://dx.doi.org/10.1016/S0277-3791(96)00007-8

Sherwood, C. R., & Creager, J. S. (1990). Sedimentary geology of the Columbia River estuary. *Progress in Oceanography, 25*, 15-79. http://dx.doi.org/10.1016/0079-6611(90)90003-K

Sherwood, C. R., Jay, D. A., Harvey, B., Hamilton, P., & Simenstad, C. A. (1990). Historical changes in the Columbia River estuary. *Progress in Oceanography, 25*, 299-352. http://dx.doi.org/10.1016/0079-6611(90)90011-P

Simenstad, C. A., Small, L. F., McIntire, C. D., Jay, D. A., & Sherwood, C. R. (1990). An introduction to the Columbia River estuary: Brief history, prior studies and the role of the CREDDP studies. *Progress in Oceanography, 25*, 1-14. http://dx.doi.org/10.1016/0079-6611(90)90002-J

Smith, N. D., Rogers, J., Aslan, A., & Blum, M. D. (2009). Contrasting styles of Holocene avulsion, Texas Gulf coastal plain, USA. In N. Smith & J. Rogers (Eds.), *Fluvial Sedimentologgy*. Blackwell Publishing Ltd., Oxford, UK.

Sundborg, A. (1956). The River Klarålven: Chapter 2. *The morphological activity of flowing water—erosion of the stream bed: Geografiska Annaler, 38*, 165-221.

Twichell, D. C., Cross, V., & Peterson, C. D. (2010). Partitioning of sediment on the shelf offshore of the Columbia River littoral cell, *Marine Geology, 273*, 11-31. http://dx.doi.org/10.1016/j.margeo.2010.02.001

USCGS. (1967). United States Coast and Geodetic Survey, Navigation Chart 6151. US Department of Commerce, Washington, D.C. Chart scale 1:40,000.

USCGS. (1968). United States Coast and Geodetic Survey, Navigation Chart 6152. US Department of Commerce, Washington, D.C. Chart scale 1:40,000.

USGS. (2013a). United States Geological Survey, SPMWave.html (2013) Fetch and Depth limited Wave Calculations. US Geological Survey Applet. Retrieved December 18, 2013, from http://woodshole.er.usgs.gov/staffpages/csherwood/sedx_equations/RunSPMWave.html

USGS. (2013b). United States Geological Survey, RunWaveCalcs.html (2013). Linear Wave Calculations. US Geological Survey Applet. Retrieved December 18, 2013, from http://woodshole.er.usgs.gov/staffpages/csherwood/sedx_equations/RunWaveCalcs.html

Vanderburgh, S., Roberts, M. C., Peterson, C. D., Phipps, J. B., & Herb, A. (2010). Holocene transgressive and regressive deposits of the Columbia River littoral cell barriers and beach plains. *Marine Geology, 273*, 32-43. http://dx.doi.org/10.1016/j.margeo.2010.02.002

Walter, S. R. (1980). *Mineralogy of the sediments of the Columbia River: the discovery of a distinctive coastal mineral* (MS Thesis, pp. 59). University of Washington, Seattle.

Wilkes, C. (1841). U.S. Ex. Ex., Columbia River, Sheets No. 1 and 2. Republished by the U.S. Department of Commerce. National Oceanic and Atmospheric Administration, National Ocean Survey. Charts 136 and 137.

Copyrights